ARTICLE IN PRESS

Transportation Research Part B xxx (xxxx) xxx

ELSEVIER

Contents lists available at ScienceDirect

Transportation Research Part B

journal homepage: www.elsevier.com/locate/trb



Platoon-centered control for eco-driving at signalized intersection built upon hybrid MPC system, online learning and distributed optimization part II: Theoretical analysis

Hanyu Zhang, Lili Du

Department of Civil and Coastal Engineering, University of Florida, Gainesville, FL 32608, United States

ARTICLE INFO

Keywords: Connected and autonomous vehicle Platoon-centered control Eco-driving strategy Model predictive control Hybrid MPC system Sequential feasibility Switching Feasibility Asymptotic stability

ABSTRACT

Extensive studies developed eco-driving strategies to smooth traffic and reduce energy consumption and emission at signalized intersections. Part I (Zhang and Du, 2022) of this study developed a novel platoon-centered control for eco-driving (PCC-eDriving), considering a mixed flow involving Connected and Autonomous Vehicles (CAVs) and Human-Driven Vehicles (HDVs). This PCC-eDriving is mathematically implemented by a hybrid Model Predictive Control (MPC) system and solved by an active-set based optimal condition decomposition algorithm (AS-OCD). It generates discrete control laws for a platoon to approach, split as sub-platoons as needed, and then pass the intersections smoothly and efficiently. Though the numerical experiments validated the effectiveness, the theoretical properties of the hybrid MPC system and the solution algorithms were not investigated. Part II of this study thus focused on these theoretical analyses. Mainly, we first analyzed and proved the MPC sequential feasibility and hybrid system switching feasibility to guarantee the control continuity of the hybrid MPC system. Next, we factored CAV control uncertainties and proved the Input-to-state stability of the robust MPC controller. These proofs theoretically ensured the effectiveness and robustness of the hybrid MPC system. Last, we proved the solution optimality and convergence of the AS-OCD algorithm. It confirmed that the AS-OCD algorithm could find the global optimal solutions for the MPC optimizers with a linear convergence rate.

1. Introduction

Input-to-State stability

Severe traffic congestion and frequent stop-and-go traffic isolation often occur around intersections with traffic lights. This non-smooth traffic pattern further causes traffic accidents (Poch and Mannering, 1996), wastes extra energy consumption and emissions (Li et al., 2014), and significantly dampens driving comfort (Summala, 2007). Inspired by recent advancements in connected and autonomous vehicle (CAV) technologies, many studies have been devoted to developing eco-driving strategies for improving traffic safety and efficiency at signalized intersections. The main idea is to inform CAVs the signal phase and timing (SPaT) through Vehicle to Infrastructure (V2I) communication technology and then plan the optimal driving strategy for CAVs to go through an intersection

DOI of original article: https://doi.org/10.1016/j.trb.2023.02.006.

Abbreviations: CAV, Connected and autonomous vehicle; MPC, Model predictive control; Eco-driving, Economic driving.

* Corresponding author.

E-mail addresses: hanyu.zhang@ufl.edu (H. Zhang), lilidu@ufl.edu (L. Du).

https://doi.org/10.1016/j.trb.2023.03.008

0191-2615/© 2023 Elsevier Ltd. All rights reserved.

Please cite this article as: Hanyu Zhang, Lili Du, Transportation Research Part B, https://doi.org/10.1016/j.trb.2023.03.008

efficiently and smoothly. Along with this thought, various eco-driving strategies have been developed, including vehicle-level constant or dynamic speed advisory (Lu and Shladover, 2014; Simchon and Rabinovici, 2020, Kamal et al., 2012; Ma et al., 2017) using heuristic or optimization approaches, or platoon-level trajectory plan (Zhao et al., 2018; Wang et al., 2019; Ma et al., 2021; Chen et al., 2021) employing platooning control to generate energy-efficient trajectory instructions. Though all of them demonstrated inspiring results, several studies (Wan et al., 2016; Ma et al., 2016, Lioris et al., 2016) indicated that vehicle-level eco-driving strategies could not guarantee system performance while platoon-level eco-driving strategies performed better in this aspect. However, developing platoon-level eco-driving strategies often need to address super difficulties in modeling and computation as involving a large-scale problem with more vehicles and considering more complex decisions such as systematically splitting a long platoon.

Our study in Part I (Zhang and Du, 2022) addressed this challenge. It developed a novel system optimal platoon-centered control for eco-driving (PCC-eDriving) at signalized intersections, leveraging CAV technologies. This PCC-eDriving is distinguished from existing platoon-level eco-driving strategies (Zhao et al., 2018; Ma et al., 2021; Chen et al., 2021) in several aspects. First, it applied a feedback closed-loop trajectory control approach rather than an open-loop trajectory planning method to improve control robustness against traffic and vehicle control uncertainties. Second, it considers the entire platoon as a system and generates optimal eco-driving control laws for the entire platoon rather than only instructing the leading CAV. In this way, the PCC-eDriving can ensure system optimality regarding traffic smoothness and energy consumption efficiency. Furthermore, the PCC-eDriving is mathematically implemented by a hybrid system, which integrates three model predictive control (MPC) controllers to respectively direct the platoon to approach, split as needed, and then pass the intersection, co-considering traffic smoothness, efficiency, and energy consumption. In particular, the hybrid MPC system uses a mixed-integer nonlinear program (MINLP) rather than heuristic approaches to break a long platoon if it cannot entirely pass the intersection in one green interval, considering traffic smoothness, traffic throughput and energy consumption. What is more, the MINLP and the optimizers of the MPC controllers are well streamlined to facilitate the control switching feasibility and efficiency. We will show this merit in our theoretical analysis later. Last, an active-set optimal condition decomposition algorithm (AS-OCD) is designed to solve the MPC controllers efficiently in a distributed computing manner.

Part I of this study (Zhang and Du, 2022) validated the effectiveness of the PCC-eDriving and the associated approaches by numerical experiments but has not yet investigated several critical issues regarding the properties of the hybrid MPC system and the solution approaches. For example, the MPC sequential feasibility, hybrid system switching feasibility, MPC control stability and AS-OCD convergence are not analyzed and proved. They together decide whether the hybrid MPC system can run smoothly and effectively. Specifically, an MPC system with sequential feasibility ensures that it can always find feasible control law that satisfies all the constraints at any future time step when it starts with an initial feasible state. The applicability of the PCC-eDriving attaches a great importance to the MPC sequential feasibility, as it significantly affects the CAV control continuity and robustness, which further impact driving safety. Built upon that, the hybrid system switching feasibility decides if the platoon under PCC-eDriving can feasibly switch from one MPC controller to another. Without this switching feasibility, the hybrid control system will fail to guide the platoon to split and pass the intersection. Furthermore, the stability of a MPC control evaluates whether and how fast the system will reach the control goal in theory. This control performance is crucial as it theoretically ensures that PCC-eDriving can quickly guide CAVs to achieve desired spacing and speed while minimizing energy consumption. Finally, the PCC-eDriving used the AS-OCD algorithm to solve the large-scale MPC optimizers in real time. The solution optimality and convergence performance of the AS-OCD algorithm significantly impact the applicability of the hybrid MPC system developed for this PCC-eDriving.

This Part II paper seeks to complete these theoretical gaps in the Part I paper. Specifically, we first analyzed and proved the MPC sequential feasibility and hybrid system switching feasibility to ensure the control continuity and smoothness of the hybrid MPC system. Then we analyzed the asymptotical stability of the MPC system and proved the Input-to-State stability of the robust MPC controller, which factors the CAV driving uncertainties. Next, this study analyzed the optimality and convergence of the AS-OCD algorithm. The theoretical analysis confirmed that the AS-OCD algorithm could quickly find the global optimal solution for the MPC controllers developed in this study with a linear convergence rate.

The effort of this study is presented by the roadmap as follows. Section 2 and 3 respectively revisits the PCC-eDriving problem setup and the hybrid MPC system. Building upon that, Section 4 analyzes and proves the sequential feasibility of the MPC controller and hybrid MPC switching feasibility. Section 5 investigates the MPC nominal system and robust system and then proves the Input-to-state

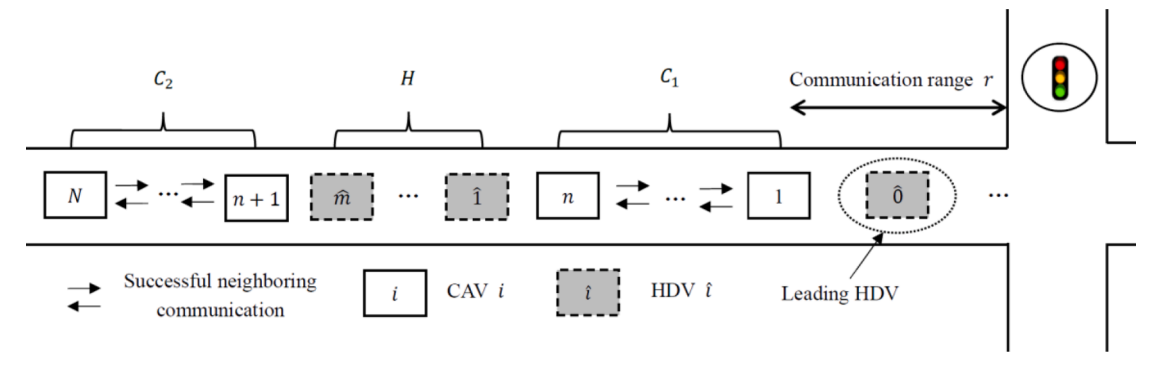


Fig. 1. Sample platoon at the signalized intersection (from part I).

Stability of the MPC controller. Furthermore, Section 6 analyzes the solution performance and proves the convergence of the AS-OCD algorithm. The whole study is summarized in Section 7.

2. PCC-edriving problem statement

This study considers a mixed-flow platoon approaching a signalized intersection on an urban road and seeks to drive it through the intersection smoothly by avoiding sharp stop/deceleration as much as possible. Using the example shown in Fig. 1, we introduce the problem setup and the notations. Without loss of generality, we consider a sample platoon involving two CAV segments sandwiched by a human-driven vehicle (HDV) segment. A longer platoon can be extended by following this pattern. Accordingly, we label the three segments as C_1 with CAVs labeled as $\{1, ..., n\}$, H with HDVs indexed by $\{\widehat{1}, ..., \widehat{m}\}$, and C_2 with CAVs labeled as $\{n+1, ..., N\}$. A CAV set $C_1 = C_2 = C_1 \cup C_2 = C$

When a platoon enters the V2I communication zoon of the traffic signal, it will receive the traffic signal phase and timing information (SPaT), including green and red phase intervals $T_g = \tau k_g$, $T_r = \tau k_r$ and remaining time of the current phase $\widetilde{T}_g = \tau \widetilde{k}_g$ or $\widetilde{T}_r = \tau \widetilde{k}_r$. Accordingly, the PCC-eDriving will instruct the platoon to split into sub-platoons as needed so that they can sequentially pass the intersection in the consecutive traffic cycles reducing sharp deceleration or stop. This control process will be conducted by a hybrid MPC system designed in Part I of our study. For completeness, we briefly introduce this hybrid system in the following section.

3. Hybrid MPC system

Mainly, the hybrid MPC system considers three states q_0, q_1, q_2 of a platoon. Correspondingly, it includes three MPC controllers MPC- q_0 , MPC- q_1 and MPC- q_2 and two switching signals σ_0, σ_1 to connect these different states and controllers. Below we specify those states and switching signals sequentially along the process of the platoon splitting and then passing an intersection.

Without loss of generality, we consider a mixed flow platoon A under state q_0 as it is driving towards a signalized intersection. The MPC- q_0 controller is then designed to conduct the car-following platooning control under state q_0 . When the platoon A enters the traffic signal communication zone, it receives the SPaT information, and then the switching signal σ_0 is triggered to determine the optimal platoon splitting plan. Specifically, a mixed-integer nonlinear program (MINLP- σ_0) is used to calculate the optimal platoon splitting point by leveraging traffic throughputs and smoothness. Following the splitting decision, the platoon A will split into two sub-platoons A_1 and A_2 . The leading sub-platoon A_1 will pass the intersection during the current green interval. We denote its state as q_1 . Whereas the latter sub-platoon A_2 cannot pass the intersection in the current signal cycle under our prediction and will be instructed to decelerate gently to avoid red idling. We denote such a state of A_2 as q_2 . Correspondingly, the MPC- q_1 and MPC- q_2 controllers are designed respectively for the states q_1 and q_2 . After the leading sub-platoon A_1 passes the intersection, the switching signal σ_1 is triggered and sub-platoon A_1 restores car-following state q_0 .

Later, when the sub-platoon A_2 reaches the communication zone, the above-mentioned procedure repeats. Specifically, the optimal platoon splitting point will be determined again and sub-platoon A_2 will further split into two sub-platoons $A_1(2)$ and $A_2(2)$ in Fig. 2. if A_2 cannot entirely pass the intersection in one green interval. Repeating this strategy, the PCC-eDriving can instruct a long platoon to pass multiple signalized intersections. In addition, the hybrid MPC is robust to accommodate unexpected accidents that causes the first sub-platoon A_1 failing to pass the intersection by splitting the A_1 further.

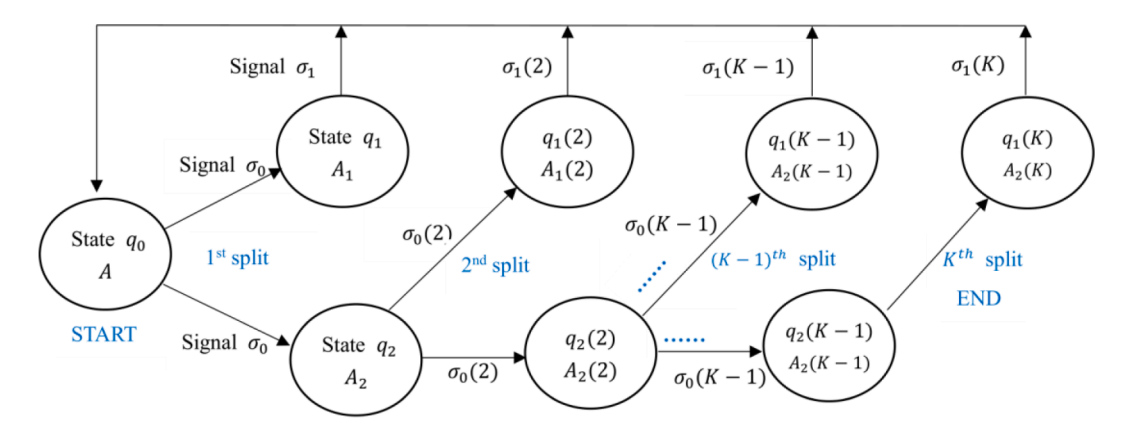


Fig. 2. Hybrid MPC system under normal traffic conditions (From Part I).

This PCC-eDriving control and the hybrid MPC system bring in technical challenges from the aspects of mathematical modeling, solution approach development, and theoretical analyses. Part I of our study have addressed the mathematical modeling and solution approach development. This Part II paper focuses on theoretical analyses and proofs regarding the control feasibility, stability and algorithm convergence. To do that, we briefly present the mathematical models of the hybrid MPC system to lay down the foundation for mathematical analyses. Please refer to Part I of our study for a detailed discussion regarding those formulations.

3.1. MPC- q_0 controller for State q_0

The MPC- q_0 controller generates the platoon-centered trajectory control laws to guide the car-following movement of CAVs in the platoon at time step $k \in \mathbb{Z}_+$ by predicting the platoon future states at any time step k+p, for $\forall p=1,...,P(p\in P)$, before it enters the traffic signal communication zone. It aims to minimize traffic oscillations and energy consumption represented by Eq. (1), subject to the vehicle dynamics and various constraints demonstrated in Eqs. (2)–(14), where the time steps in the prediction horizon is denoted as k_P . Hereafter, we also simplify step k+p to p throughout this section to avoid complex notation.

 $MPC-q_0$

$$\mathbf{Min} \ \Gamma(u(p)) = \sum_{p=1}^{P} \left\{ \frac{1}{2} \left[z^{T}(p) Q_{z} z(p) + (z'(p))^{T} Q_{z'} z'(p) \right] + \frac{\tau^{2}}{2} \omega_{1} \| \ u(p-1) \|_{2}^{2} \right\}$$
 (1)

Subject to

$$x_i(k+1) = x_i(k) + \tau v_i(k) + \frac{\tau^2}{2} (u_i(k) - \Delta u_i(k)), \ i \in I_C, \ k \in k_p$$
 (2)

$$v_i(k+1) = v_i(k) + \tau(u_i(k) - \Delta u_i(k)), \ i \in I_C, \ k \in k_p$$
(3)

$$\Delta u_i(k) = \varepsilon_i v_i(k) + \eta_i u_i(k) - \eta_i u_i(k-1), \ i \in I_C, \ k \in k_p$$

$$\tag{4}$$

$$x_{\hat{n}}(k) = x_n(k - T_{\hat{m}}) - D_{\hat{m}}, \ k \in k_p$$
 (5)

$$a_{min,i} \le u_i(k) \le a_{max,i}, \ i \in I_C, \ k \in k_p$$
 (6)

$$v_{min} \le v_i(k) \le v_{max}, \ i \in I_C, \ k \in k_p \tag{7}$$

$$x_{i-1}(k) - x_i(k) > L_i + \delta_1 \tau v_i(k) + \delta_2 \tau (v_i(k) - v_{i-1}(k)), i \in I_C, k \in k_n$$
 (8)

$$s_i(k) = L_i + \delta_1 \tau v_i(k) + \delta_2 \tau(v_i(k) - v_{i-1}(k)) + \delta, \ i \in I_C, \ k \in k_p$$
 (9)

$$\Delta x_i(k) = x_{i-1}(k) - x_i(k) - s_i(k), \ i \in I_C, \ k \in k_p$$
(10)

$$\Delta v_i(k) = v_{i-1}(k) - v_i(k), \ i \in I_C, \ k \in k_p$$
(11)

$$z(k) := (\Delta x_1(k), \dots, \Delta x_N(k))^T \in \mathbb{R}^N, \ k \in k_n$$

$$(12)$$

$$z'(k) := (\Delta v_1(k), ..., \Delta v_N(k))^T \in \mathbb{R}^N, \ k \in k_n$$
 (13)

$$\Phi_f := (z(k+P) \in \zeta, z'(k+P) \in \zeta'). \tag{14}$$

More exactly, Eqs. (2)–(4) represent the robust CAV dynamics using double integrator model. $\Delta u_i(k)$ represents the CAV i's control uncertainties including powertrain delay and aerodynamic drag etc. Eq. (5) uses Newell's car-following model Newell, 2002) to predict HDV driving behaviors. Eqs. (6)–(8) respectively illustrate the acceleration, speed limits and safe distance constraints of CAV i. Eq. (9) describes the desired spacing policy for CAV i, Eqs. (10)–(11) curve the spacing and speed tracking errors of CAV i. Accordingly, the tracking errors of all the CAVs together form the platoon tracking dynamics in Eqs. (12)–(13). Finally, Eq. (14) presents the terminal constraints. It requires the platoon spacing and speed tracking errors will be confined to small domains ζ and ζ' respectively at final time step k+P of the MPC prediction horizon. It should be noted that this study employed Newell's car-following model for friendly computation performance (see the justification given in Section 3 in Part I). Nevertheless, replacing Newell with other math complicated car-following models such as Wiedemann Wiedemann, 1991) or IDM (Treiber et al., 2000) models will not affect the MPC recursive feasibility and stability for the following reasons. First of all, the HDV car-following model is served as equality constraints in Eq. (5) in MPC, so that it will not affect MPC sequential feasibility given the initial state is satisfied (see the proofs in section 4 later). And the MPC stability proof in section 5 later is only related to CAV dynamics in Eqs. (2)–(4), terminal constraints in Eq. (14) and cost function in Eq. (1) according to Mayne et a., (2000). Hence, it will also not affect the MPC stability in this paper.

Note that this platoon-centered car-following control is different from the existing approach in Gong et al., (2016); Gong and Du, (2018); Shen et al., (2021). It explicitly factors the CAV control uncertainties by Eq. (4), HDV driving variations by Eq. (5) as well as adaptive safe distance constraints and desired spacing policy by Eqs. (8) and (9). These enhanced features capture more traffic and

control reality, aiming to improve the traffic system performance in urban environments, but introduce extra challenges in the MPC sequential feasibility and control stability. We will address these challenges in Section 4 and Section 5.

3.2. Switching signal MINLP- σ_0

The MINLP- σ_0 optimizer determines the optimal splitting point and triggers the switching signal σ_0 in the hybrid MPC system. The splitting decision tries to balance traffic throughput and smoothness represented by the objective function in Eq. (15) subject to the same vehicle dynamics and safety constraints used in MPC- q_0 while considering extra constraints regarding the splitting point in Eqs. (16)–(21). This way, we can ensure the optimal split point can be successfully implemented while sustaining control switching feasibility. We will discuss it in section 4.

MINLP- σ_0

$$\min J(u, y) = J_1(u, y) + \omega_2 J_2(u, y) \tag{15}$$

where

$$J_{1}(u,y) = \sum_{p=1}^{P=\bar{k}_{g}+k_{r}} \left\{ \frac{1}{2} \left[z^{T}(p) Q_{z} z(p) + (z^{'}(p))^{T} Q_{z^{'}} z^{'}(p) \right] + \frac{\tau^{2}}{2} \omega_{1} \| u(p-1) \|_{2}^{2} \right\}$$

$$J_2(u,y) = -\sum_{i \in \overline{I_c}} i * y_i$$

Subject to constraints in Eqs. (2)–(9), (12)–(13), (16)–(21):

$$\sum_{i \in \overline{I_c}} y_i = 1; y_i \in \{0, 1\}, \ i \in \overline{I_c}$$
 (16)

Eq. (16) requires only one splitting point exits in the platoon, where y_i is a binary variable to describe the location of the platoon splitting point. For instance, y_i = 1 represents that the platoon splits ahead of CAV i^* .

$$x_{i-1}(\overline{k}_g) \ge -M(1-y_i), \ i \in \overline{I_c},\tag{17}$$

Eq. (17) predicts the last CAV i^*-1 in the first sub-platoon A_1 can pass the intersection before the end of the current green interval at time step $p=\widetilde{k}_g$. It requires the splitting decision made by the MINLP- σ_0 model can ensure the A_1 can entirely pass the intersection in the current green interval.

$$x_i(\widetilde{k}_g + k_r) \le M(1 - y_i), \ i \in \overline{I}_c, \tag{18}$$

On the other hand, Eq. (18) predicts the movement of the second sub-platoon A_2 after splitting. It requires the splitting decision made by the MINLP- σ_0 model should consider that the sub-platoon A_2 cannot pass the intersection until the end of the sequential red interval at time step $p = \tilde{k}_s + k_r$.

$$i * v_i < C, i \in \overline{I_C}.$$
 (19)

Next, Eq. (19) indicates the splitting decision is constrained by the downstream traffic capacity, where C represents the number of vehicles allowed to pass the intersection based on the current downstream traffic condition.

$$\Delta x_i(p) = x_{i-1}(p) - x_i(p) - s_i(p) - y_i * \mathcal{D}, \ i \in \overline{I_c},$$

$$\tag{20}$$

$$\Delta v_i(p) = v_{i-1}(p) - v_i(p) - v_i * \mathscr{D}', \ i \in \overline{I_c}, \tag{21}$$

Finally, Eqs. (20)–(21) factor the future platoon spacing and speed errors $\mathscr D$ and $\mathscr D$ at the splitting point.

Overall, the MINLP- σ_0 will find the optimal platoon splitting point by predicting the future platoon control and movements during the current green and sequential red intervals, namely the next $P = \tilde{k}_g + k_r$ time steps. It will guide the followed MPC- q_1 and MPC- q_2 control and help to ensure the feasibility of the state switching $q_0 \stackrel{\sigma_0}{\rightarrow} (q_1, q_2)$. We will discuss these details in Section 4.

3.3. MPC- q_1 controller for state q_1

The MPC- q_1 controller instructs a sub-platoon, e.g., A_1 , under state q_1 to efficiently and smoothly pass the intersection in the current green interval. For discussion convenience, we use $\widehat{A_1}$ to denote the CAV set in sub-platoon A_1 , and formally present MPC- q_1 below. \mathbf{MPC} - q_1

$$Min \ \Gamma(u) = \sum_{p=1}^{P} \left\{ \frac{1}{2} \left[z^{T}(p) Q_{z} z(p) + (z'(p))^{T} Q_{z'} z'(p) \right] + \frac{\tau^{2}}{2} \omega_{1} u(p-1) \right\}$$
 (22)

H. Zhang and L. Du

Subject to, for $i \in \widehat{A}_1, p \in P$ where $P = \widetilde{k}_g, \ \widetilde{k}_g - 1, ..., 1$: Constraints in Eqs. (2)–(13), and

$$x_{i^*-1}(P) \ge 0,$$
 (23)

Eq. (23) ensures that the sub-platoon A_1 passes the intersection within the remaining green interval. It is derived from Eq. (17) in the MINLP- σ_0 . To keep control continuity and facilitate switching feasibility, MPC- q_1 also shares the same constraints in Eqs. (2)–(13) with MPC- q_0 . We will discuss these technical details to ensure switching feasibility in section 4.

3.4. MPC- q_2 controller for state q_2

Last, MPC- q_2 controller instructs a sub-platoon (e.g., A_2) under state q_2 to split and smoothly approach the intersection while reducing sharp deceleration and red idling. In general, MPC- q_2 can have two controllers, including MPC- q_2 -(i) that generates its ecodriving trajectory for the leading CAV i^* in A_2 , and (ii) MPC- q_2 -(ii) that generates system optimal car-following control laws for all other CAVs in A_2 following the leading CAV i^* .

MPC- q_2 -(i) Eco-driving Trajectory Reference of Leading CAV i^* .

$$\mathbf{Min} \ \mathbf{F}(u_{i^*}) = \sum_{p=1}^{p} \| \ u_{i^*}(p-1) \|_2^2 - \omega_3 x_{i^*}(P)$$
 (24)

Subject to, for $p \in P$, $P = \widetilde{k}_g + k_r$, $\widetilde{k}_g + k_r - 1$, ..., 1:

CAV i^* dynamics and constraints in Eqs. (1)–(3) and (6)–(8).

$$x_{i^*}(P) \le 0, \tag{25}$$

The objective function in Eq. (24) tunes the parameter ω_3 to balance the two conflict objectives in minimizing energy consumption and maximizing traffic throughputs. Eq. (25) presents that the CAV i^* won't pass the intersection during the red interval according to the splitting decision from MINLP- σ_0 . It also indirectly avoids the following vehicles running the red light.

MPC-*q*₂**-(ii)** Following Vehicles' Trajectory Control.

$$\mathbf{Min} \ \Gamma(u) = \sum_{p=1}^{P} \left\{ \frac{1}{2} \left[z^{T}(p) Q_{z} z(p) + (z'(p))^{T} Q_{z'} z'(p) \right] + \frac{\tau^{2}}{2} \omega_{1} \| \ u(p-1) \|_{2}^{2} \right\}$$
(26)

Subject to, for $i \in \widehat{A_2} \setminus i^*$, $p \in P$ where $P = \widetilde{k_g} + k_r$, $\widetilde{k_g} + k_r - 1$, ..., 1: Constraints in Eqs. (2)–(13),

Here, we use $\widehat{A_2}$ to denote the CAV set in the sub-platoon A_2 . The MPC- q_2 -(ii) is a system optimal car-following control to guide the sub-platoon A_2 to smoothly follow the leading eco-driving trajectory reference provided by the MPC- q_2 -(i). To ensure the hybrid MPC system switching feasibility, the MPC- q_2 -(ii) controller is designed to be very similar to MPC- q_0 except a shrinking prediction horizon P.

4. Feasibility of the hybrid MPC system

We first investigate three important properties of the hybrid MPC system: sequential feasibility, hybrid system switching feasibility, and MPC terminal constraint feasibility. They together ensure the control continuity and smoothness of the hybrid MPC system.

4.1. MPC sequential feasibility

MPC is implemented recursively at each time step 0, 1, ..., k-1, k. Therefore, a fundamental theoretical question is whether the MPC can find a feasible control law at each time step k (i.e., whether the constraint set of the MPC optimizer is non-empty at each time step k), given the platoon system starts from an initial feasible condition at k=0. A MPC system is called sequential (recursive) feasible Löfberg, 2012) if the answer to this question is affirmative. The hybrid MPC system in this study has three controllers: MPC- q_0 , MPC- q_1 and MPC- q_2 . MPC- q_0 has constraints in Eqs. (2)–(14), which are also shared with MPC- q_1 and MPC- q_2 except the terminal constraint in Eq. (14). Hence, this study first proves the sequential feasibility of MPC- q_0 . Then, we further discuss the sequential feasibility of MPC- q_1 and MPC- q_2 as well as the switching feasibility of the hybrid system in Section 4.2. To prove the sequential feasibility of the MPC- q_0 , we first classify Eqs. (2)–(14) into the following three sets:

- (i) $\mathscr{S}_1(u(k))$: constraint set in Eqs. (2)–(4) and (6)–(8) for capturing the CAV dynamics, acceleration, speed and safety constraints at step $k \in \mathbb{Z}_+$.
- (ii) $\mathcal{S}_2(u(k), Z(k+P))$: the HDV movements in Eq. (5) and the terminal constraint in Eq. (14) at step $k \in \mathbb{Z}_+$.
- (iii) $\mathcal{S}_3(u(k))$: the control dynamics in Eqs. (9)–(13) at step $k \in \mathbb{Z}_+$.

It should be noticed that the third constraint set $\mathcal{S}_3(u(k))$ involves control dynamic formulations. They are always feasible if the first constraint set $\mathcal{S}_1(u(k))$ is feasible. For the second constraint set $\mathcal{S}_2(u(k), Z(k+P))$, Eq. (5) is an equality constraint to curve the

HDV trajectory. Thus, they are always feasible in math and also stay feasible in practice if accurate time and distance displacements are estimated. Apart from it, the terminal constraint in Eq. (14) is only active at the final time step k + P of the MPC. Its sequential feasibility is ensured if the nominal MPC system is asymptotical stable (see proof in detail in Section 5.2) according to Mayne et al., (2000). Consequently, to prove the sequential feasibility of the MPC- q_0 , this study will mainly analyze and prove the sequential feasibility of the first constraint set $\mathcal{S}_1(u(k))$ by Lemma 1.

Lemma 1. For $k \in \mathbb{Z}_+ := \{0, 1, 2, ...\}$ and $i \in I_C$, if $\mathscr{S}_1(u_i(k))$ is feasible, then there exists $\delta_1 \ge 1$ and $\delta_2 \ge 0$ that make $\mathscr{S}_1(u_i(k+1))$ feasible and compact. In addition, the non-empty feasible control input profile $\mathbb{S}_1(u_i(k))$ for platoon vehicle i at step k is given below:

$$u_i(k) \in \mathbb{S}_1(u_i(k)) = \left[\max \left\{ a_{\min,i}, \underline{a_{i,v}} \right\}, \min \left\{ a_{\max,i}, \overline{a_{i,d}} \right\} \right], \tag{27}$$

where

$$\underline{a_{i,v}} = \frac{v_{min} - (1 - \tau \varepsilon_i)v_i(k) - \tau \eta_i u_i(k-1)}{\tau (1 - \eta_i)} \le 0$$

$$\overline{a_{i,v}} = \frac{v_{max} - (1 - \tau \varepsilon_i)v_i(k) - \tau \eta_i u_i(k-1)}{\tau (1 - \eta_i)} \ge 0$$

$$\overline{a_{i,d}} = \varepsilon_i v_i(k) + \eta_i u_i(k) - \eta_i u_i(k-1) + \frac{g_i(k) + \tau(v_{i-1}(k+1) - v_i(k))}{\tau^2 \left(\delta_1 + \delta_2 + \frac{1}{2}\right)} + \frac{\left(\delta_2 - \frac{1}{2}\right) u_{i-1}(k)}{\delta_1 + \delta_2 + \frac{1}{2}}$$

$$g_i(k) = x_{i-1}(k) - x_i(k) - (L_i + \delta_1 \tau v_i(k) + \delta_2 \tau (v_i(k) - v_{i-1}(k)))$$

Proof: To prove the sequential feasibility of the constraint set $\mathscr{S}_1(u_i(k))$ constituted of Eqs. (2)–(4) and (6)–(8), we need to find a non-empty control input profile $\mathbb{S}_1(u_i(k))$ at step k for $k \in \mathbb{Z}_+$ that makes the constraint set $\mathscr{S}_1(u_i(k+1))$ feasible, given that $\mathscr{S}_1(u_i(k))$ is feasible. Namely, with feasible state at any step k, the MPC can have a feasible control input at step k leading to a feasible state at step k+1. Below we provide the technical details.

We first reformulate the speed limit constraint at step k+1 according to Eqs. (3), (4) and (7). And then we find its corresponding feasible control input set $u_i(k) \in \left[a_{i,v}, \overline{a_{i,v}}\right]$ as follows in Eq. (28).

$$v_{min} \leq v_{i}(k+1) \leq v_{max}$$

$$\Leftrightarrow v_{min} \leq v_{i}(k) + \tau(u_{i}(k) - \Leftrightarrow u_{i}(k)) = v_{max}$$

$$\Leftrightarrow v_{min} \leq (1 - \tau \varepsilon_{i})v_{i}(k) + \tau(1 - \eta_{i})u_{i}(k) + \tau \eta_{i}u_{i}(k-1) \leq v_{max}$$

$$\Leftrightarrow u_{i}(k) \in \left[a_{i,v}, \overline{a_{i,v}}\right],$$
(28)

where the lower bound $a_{i,v}$ and upper bound $\overline{a_{i,v}}$ are given in Eq. (29).

$$\underline{a_{i,v}} = \frac{v_{min} - (1 - \tau \varepsilon_i)v_i(k) - \tau \eta_i u_i(k-1)}{\tau (1 - \eta_i)}$$

$$\underline{a_{i,v}} = \frac{v_{max} - (1 - \tau \varepsilon_i)v_i(k) - \tau \eta_i u_i(k-1)}{\tau (1 - \eta_i)}$$
(29)

Similarly, we reformulate the safe distance constraints at step k+1 according to Eqs. (2)–(4) and (8). For discussion convenience, we use $g_i(k)$ to represent the safe distance constraint in Eq. (8) for CAV i at step k and denote $\underline{u_i(k)} = u_i(k) - \Delta u_i(k)$. Then, we present the mathematical derivations below in Eq. (30).

$$g_{i}(k+1) = x_{i-1}(k+1) - x_{i}(k+1) - (L_{i} + \delta_{1}\tau v_{i}(k+1) + \delta_{2}\tau(v_{i}(k+1) - v_{i-1}(k+1)))$$

$$= x_{i-1}(k) - x_{i}(k) + \tau(v_{i-1}(k) - v_{i}(k)) + \frac{\tau^{2}}{2} \left(\underline{u_{i-1}(k)} - \underline{u_{i}(k)} \right)$$

$$-(L_{i} + \delta_{1}\tau v_{i}(k) + \delta_{2}\tau(v_{i}(k) - v_{i-1}(k))) - \delta_{1}\tau^{2}\underline{u_{i}(k)} - \delta_{2}\tau^{2} \left(\underline{u_{i}(k)} - \underline{u_{i-1}(k)} \right)$$

$$= g_{i}(k) + \tau(v_{i-1}(k) - v_{i}(k)) + \tau^{2} \left(\delta_{2} + \frac{1}{2} \right) \underline{u_{i-1}(k)} - \tau^{2} \left(\delta_{1} + \delta_{2} + \frac{1}{2} \right) \underline{u_{i}(k)}$$

$$= g_{i}(k) + \tau(v_{i-1}(k+1) - v_{i}(k)) + \tau^{2} \left(\delta_{2} - \frac{1}{2} \right) \underline{u_{i-1}(k)} - \tau^{2} \left(\delta_{1} + \delta_{2} + \frac{1}{2} \right) \underline{u_{i}(k)}$$

$$= g_{i}(k) + \tau(v_{i-1}(k+1) - v_{i}(k)) + \tau^{2} \left(\delta_{2} - \frac{1}{2} \right) \underline{u_{i-1}(k)} - \tau^{2} \left(\delta_{1} + \delta_{2} + \frac{1}{2} \right) \underline{u_{i}(k)}$$

Note that we assume $\mathscr{S}_1(u_i(k))$ is feasible, it makes the safe distance constraints in Eq. (8) feasible at time step k. Mathematically, $g_i(k) \ge 0$. To make the safe distance constraints keep feasible at next time step k+1 (i.e., $g_i(k+1) \ge 0$), we should have the following control input requirement $(u_i(k) \le \overline{a_{id}})$ in Eq. (31) based upon Eqs. (4) and (30).

$$u_i(k) \leq \overline{a_{i,d}} = \varepsilon_i v_i(k) + \eta_i u_i(k) - \eta_i u_i(k-1)$$

$$+\frac{g_{i}(k)+\tau(v_{i-1}(k+1)-v_{i}(k))}{\tau^{2}\left(\delta_{1}+\delta_{2}+\frac{1}{2}\right)}+\frac{\left(\delta_{2}-\frac{1}{2}\right)\underline{u_{i-1}(k)}}{\delta_{1}+\delta_{2}+\frac{1}{2}}\tag{31}$$

Recall that we define $\delta_1 \geq 1$, $\delta_2 \geq 0$ for Eq. (8). Without loss of generalizability, we pick $\delta_1 \geq \max\left\{\frac{v_{min}-v_{max}}{\tau(a_{min,i}-\epsilon v_{min})}-1, 1\right\}$, $\delta_2 = \frac{1}{2}$ to show the sequential feasibility¹. By plugging in $\delta_2 = \frac{1}{2}$, we can remove the term with $u_{i-1}(k)$ and simplify Eq. (31) to Eq. (32) below.

$$\overline{a_{i,d}} = \varepsilon_i v_i(k) + \eta_i u_i(k) - \eta_i u_i(k-1) + \frac{g_i(k) + \tau(v_{i-1}(k+1) - v_i(k))}{\tau^2(\delta_i + 1)}$$
(32)

Wrapping the Eqs. (6), (28), (31) and (32), we have the following solution set $\mathbb{S}_1(u_i(k))$ in Eq. (33) that makes the constraints set $\mathscr{S}_1(u_i(k+1))$ feasible given that $\mathscr{S}_1(u_i(k))$ is feasible.

$$u_i(k) \in \mathbb{S}_1(u_i(k)) = \left[\max \left\{ a_{\min,i}, \underline{a_{i,v}} \right\}, \min \left\{ a_{\max,i}, \overline{a_{i,v}}, \overline{a_{i,d}} \right\} \right]$$

$$(33)$$

We next show $\mathbb{S}_1(u_i(k))$ in Eq. (33) is non-empty. To do that, it suffices to show $\max\left\{a_{min,i},\underline{a_{i,v}}\right\} \leq \min\left\{a_{max,i},\overline{a_{i,v}},\overline{a_{i,d}}\right\}$. More specifically, we need to prove the following six inequalities hold (i) $a_{max,i} \geq a_{min,i}$, (ii) $a_{max,i} \geq \underline{a_{i,v}}$, (iii) $\overline{a_{i,v}} \geq a_{min,i}$, (iv) $\overline{a_{i,v}} \geq \underline{a_{i,v}}$, (v) $\overline{a_{i,d}} \geq \underline{a_{i,v}}$, It is obvious that (i) $a_{max,i} \geq a_{min,i}$ and (iv) $\overline{a_{i,v}} \geq \underline{a_{i,v}}$ hold according to Eqs. (6) and (29). Below we sequentially show the inequalities (ii), (iii), (v), and (vi) are satisfied in the Eqs. (34)–(37) when $\delta_1 \geq \max\left\{\frac{v_{min}-v_{max}}{\tau(a_{min,i}-\varepsilon v_{min})}-1, 1\right\} \geq \frac{v_{min}-v_{max}}{\tau(a_{min,i}-\varepsilon v_{min})}-1$ and $\delta_2 = \frac{1}{2}$.

Specifically, we confirm inequality (ii) $a_{max,i} \ge a_{i,v}$ holds by the derivations given in Eq. (34).

$$a_{max,i} - \underline{a_{i,v}} = a_{max,i} - \frac{v_{min} - (1 - \tau \varepsilon_i)v_i(k) - \tau \eta_i u_i(k - 1)}{\tau (1 - \eta_i)} \ge a_{max,i} + \frac{-v_{min} + (1 - \tau \varepsilon_i)v_{min} + \tau \eta_i a_{min,i}}{\tau (1 - \eta_i)} = a_{max,i} - \frac{\varepsilon_i v_{min} - \eta_i a_{min,i}}{(1 - \eta_i)} > 0$$
(34)

We prove inequality (iii) $\overline{a_{i,v}} \ge a_{min,i}$ by the mathematical process in Eq. (35).

$$\overline{a_{i,v}} - a_{min,i} = \frac{v_{max} - (1 - \tau \varepsilon_i)v_i(k) - \tau \eta_i u_i(k-1)}{\tau (1 - \eta_i)} - a_{min,i} \ge \frac{v_{max} - (1 - \tau \varepsilon_i)v_{max} - \tau \eta_i a_{max,i}}{\tau (1 - \eta_i)} - a_{min,i} = \frac{\varepsilon_i v_{max} - \eta_i a_{max,i}}{(1 - \eta_i)} - a_{min,i} > 0$$
 (35)

To ensure inequality (v) $\overline{a_{id}} > a_{min,i}$, we develop the mathematical process in Eq. (36).

$$\begin{split} \overline{a_{i,d}} - a_{\min,i} &= \frac{\varepsilon_{i} v_{i}(k) - \eta_{i} u_{i}(k-1)}{(1-\eta_{i})} + \frac{g_{i}(k) + \tau(v_{i-1}(k+1) - v_{i}(k))}{\tau^{2}(\delta_{1}+1)(1-\eta_{i})} - a_{\min,i} \\ &\geq \frac{1}{(1-\eta_{i})} \left[\frac{v_{i-1}(k+1) - v_{i}(k)}{\tau(\delta_{1}+1)} - (1-\eta_{i})a_{\min,i} + (\varepsilon_{i}v_{i}(k) - \eta_{i}u_{i}(k-1)) \right] + \frac{g_{i}(k)}{\tau^{2}(\delta_{1}+1)(1-\eta_{i})} \\ &\geq \frac{1}{(1-\eta_{i})} \left[\frac{v_{\min} - v_{\max}}{\tau(\delta_{1}+1)} - (1-\eta_{i})a_{\min,i} + (\varepsilon_{i}v_{\min} - \eta_{i}a_{\min,i}) \right] = \frac{1}{(1-\eta_{i})} \left[\frac{v_{\min} - v_{\max}}{\tau(\delta_{1}+1)} - (a_{\min,i} - \varepsilon_{i}v_{\min}) \right] \end{split}$$
(36)

By choosing a feasible $\delta_1 \geq \frac{\nu_{\min} - \nu_{\max}}{\tau(a_{\min,l} - \varepsilon \nu_{\min})} - 1$, we have $\frac{1}{(1-\eta_i)} \left[\frac{\nu_{\min} - \nu_{\max}}{\tau(\delta_1 + 1)} - (a_{\min,l} - \varepsilon_i \nu_{\min}) \right] \geq 0$. Consequently, we confirm inequality (v) $\overline{a_{i,d}} - a_{\min,i} \geq 0$ in Eq. (36).

Last, we confirm inequality (v) $\overline{a_{i,d}} \ge a_{min,i}$ by the derivation below in Eq. (37).

$$\overline{a_{i,d}} - \underline{a_{i,v}} = \left[\frac{\varepsilon_{i}v_{i}(k) - \eta_{i}u_{i}(k-1)}{(1 - \eta_{i})} + \frac{g_{i}(k) + \tau(v_{i-1}(k+1) - v_{i}(k))}{\tau^{2}(\delta_{1} + 1)(1 - \eta_{i})} \right] - \frac{v_{min} - (1 - \tau\varepsilon_{i})v_{i}(k) - \tau\eta_{i}u_{i}(k-1)}{\tau(1 - \eta_{i})} \\
> \frac{1}{\tau(1 - \eta_{i})} \left[\frac{v_{i-1}(k+1) - v_{i}(k)}{\delta_{1} + 1} - (v_{min} - v_{i}(k)) \right] = \frac{v_{i-1}(k+1) - v_{min} + \delta_{1}(v_{i}(k) - v_{min})}{\tau(1 - \eta_{i})(\delta_{1} + 1)} \ge 0$$
(37)

Wrapping the results above, we prove the sequential feasibility of the constraints $\mathcal{S}_1(u(k))$, with which we conclude Lemma 1.

4.2. Hybrid switching feasibility

Built upon the sequential feasibility of each MPC, switching feasibility guarantees that MPC controllers in a hybrid system can feasibly switch according to the hybrid system design. Then to ensure the continuity of the hybrid system, it is crucial to prove the switching feasibility (Mhaskar, et al., 2005). Namely, the system can keep feasible as the control switches from one MPC controller to another. As shown in Fig. 2, the hybrid system of this study involves three types of state switching: (i) $q_0 \stackrel{\sigma_0}{\rightarrow} q_1$, q_2 ; (ii) $q_1 \stackrel{\sigma_1}{\rightarrow} q_0$; (iii) $q_2(\kappa-1) \stackrel{\sigma_0}{\rightarrow} q_1(\kappa)$, $q_2(\kappa)$. Given the sequential feasibility of MPC- q_0 proved in Section 4.1, we show the switching feasibility one by one

¹ Please note that the selection of the parameters here is to ensure feasibility rigorously. It is not necessarily the best choice for the implementation.

below.

- (i) $q_0 \stackrel{\sigma_0}{\to} q_1$, q_2 represents the platoon A under the control of MPC- q_0 splits into two sub-platoons A_1 and A_2 by switching signal σ_0 , and then operate respectively under the control of MPC- q_1 and MPC- q_2 . Note that MPC- q_1 and MPC- q_2 share the same vehicle dynamics and constraints in Eqs. (2)–(14) with MPC- q_0 except extra constraints in Eqs. (23) and (25). Therefore, the control switching feasibility is ensured if MPC- q_1 and MPC- q_2 stay sequential feasible with these extra constraints. To demonstrate it, recall that the switching signal MINLP σ_0 also shares the same vehicle dynamics and constraints in Eqs. (2)–(14) with MPC- q_0 , while Eq. (23) in MPC- q_1 and (25) in MPC- q_2 are respectively derived from Eqs. (17) and (18) in the MINLP- σ_0 . That is to say, if MINLP- σ_0 can find a feasible platoon splitting point factoring Eqs. (17) and (18), then involving constraints in Eqs. (23) or (25) into MPC- q_0 for switching to MPC- q_1 or MPC- q_2 (i.e., implementing splitting point decision in the MPC control) will ensure that MPC- q_1 and MPC- q_2 can always find feasible trajectory control solution at each step (i.e., the sequential feasibility of MPC- q_1 and MPC- q_2 is confirmed). According to the definition of the platoon splitting point in Eq. (16), MINLP- σ_0 can always find a feasible platoon splitting point. Therefore, we confirm the sequential feasibility of MPC- q_1 and MPC- q_2 and the switching feasibility of $q_0 \stackrel{\sigma_0}{\to} q_1$, q_2 .
- (ii) $q_1 \stackrel{\sigma_1}{\to} q_0$ represents the control of the sub-platoon A_1 switches from MPC- q_1 to MPC- q_0 when the switching signal σ_1 is triggered. Note that the MPC- q_0 has an extra terminal constraint in Eq. (14) compared with MPC- q_1 . If the terminal constraint in Eq. (14) is always feasible, then the switching $q_1 \stackrel{\sigma_1}{\to} q_0$ is feasible. Recall that the terminal constraint in Eq. (14) regulates the platoon control error to be limited in a defined range at the end of the prediction horizon P. It is always feasible when the prediction horizon P is large enough (see section 4.3). Therefore, the feasibility of this switching is ensured.
- (iii) $q_2(\kappa-1) \xrightarrow{\sigma_0(\kappa)} q_1(\kappa)$, $q_2(\kappa)$ represents the sub-platoon $A_2(\kappa-1)$ under the control of MPC- $q_2(\kappa-1)$ further splits into the sub-platoon $A_1(\kappa)$ under the control of MPC- $q_2(\kappa)$ when switching signal $\sigma_0(\kappa)$ is triggered. Similar to the first type of switching, MPC- $q_1(\kappa)$ and MPC- $q_2(\kappa)$ share the same vehicle dynamics and constraints with MPC- $q_2(\kappa-1)$, but have extra constraints in Eqs. (23) and (25). The switching feasibility is ensured according to the same discussion for (i) $q_0 \xrightarrow{\sigma_0} q_1$, q_2 .

Overall, the discussions above ensure the sequential feasibility of MPC- q_1 and MPC- q_2 and also guarantee the feasibility of the state switchings in the well-designed hybrid system.

4.3. MPC terminal constraint feasibility

The MPC- q_0 introduces the terminal constraints in Eq. (14) to facilitate the MPC stability. Specifically, Eq. (14) requires all CAVs in the platoon to reach a steady state at the end of the prediction horizon P, namely, the spacing and speed tracking errors are confined to small domains at step P. Intuitively, if the MPC prediction horizon P is too small, the platoon may not have enough time to adjust spacing and speed and satisfy Eq. (14). On the other side, if P is set vary large, it introduces tremendous computation loads, though the terminal constraint in Eq. (14) becomes feasible. Hence, the problem becomes how to theoretically quantify the minimum P value to ensure Eq. (14) feasible while reducing the computation loads.

The rigorous analysis of the minimum P value is not trivial because the movements of the CAVs are constrained by acceleration/speed limits in Eq. (6)–(7) and coupled and constrained by safe distance constraints in Eq. (8). To tackle the problem, we construct a series of feasible driving strategies to make vehicles sequentially satisfy the terminal constraint in Eq. (14). Mainly, we first make the leading CAV satisfy its terminal constraint in Eq. (14) using feasible control strategies that satisfy constraints in Eqs. (2)–(13), then the second CAV, the third CAV, ..., until the last CAV in the platoon. With this idea in mind, we consider a simple case E where only two CAVs are involved. We make the leading CAV stay a constant speed and manage the following CAV to reach the same speed and desired spacing as the leading CAV in P_E time steps using the well-designed vehicle driving strategy E0. As such, we figure out it needs E1 time steps for one CAV to reach steady-state and satisfy terminal constraint in Eq. (14). It is noted that E1 is related with CAVs' initial states and acceleration/speed limits.

Next, we extend this two-CAV simple case E to a general case with n CAVs, by letting CAVs sequentially implement the strategy s in the order from the first to the last vehicle in the platoon. Then the corresponding number of time steps needed is $\sum_{i=1}^{n} P_{E}(i)$ for the general n-vehicle case. In summary, $\sum_{i=1}^{n} P_{E}(i)$ provides a lower bound for the MPC prediction horizon P. If the MPC prediction horizon $P \ge \sum_{i=1}^{n} P_{E}(i)$, the MPC terminal constraint feasibility is ensured.

Our analyses and proofs indicated that the lower bound value of P (i.e., $\sum_{i=1}^{n} P_{E}(i)$) highly depends on the platoon size n and each CAV $P_{E}(i)$ value, which is further related with CAVs' initial states and acceleration/speed limits. As the platoon size increases, or the CAVs' initial states move further away from the steady-state, or the feasible acceleration/speed ranges get smaller, the lower bound value $\sum_{i=1}^{n} P_{E}(i)$ theoretically increases. In practice, if the platoon is initially close to the steady-state (e.g., $\pm 5m$ from desired spacing,

 \pm 2 (m/s) from desired speed), then P=15 is large enough to ensure the terminal constraints in Eq. (14) feasible for a platoon with 10 CAVs. To factor in the traffic signal phase and timing information, this study set P to be at least 20 or even 30, which ensured the feasibility of the terminal constraints in most scenarios for a reasonable platoon size.

The entire proof involves many scenarios regarding CAVs' initial states and acceleration/speed limits, which make the proof itself tedious and very lengthy. In addition, the proof is similar to the feasibility proof developed in our previous work (Zhang et al., 2022).

Thus, we omit the detailed proofs in this study but put them on arXiv (Zhang and Du, 2022).

5. MPC control stability

This section studies the control stability of the MPC controllers. The control stability plays a vital role in ensuring the system's performance. It theoretically guarantees that the platoon system can go to the desired spacing and speed even when exposed to disturbances. A system fails to reach or sustain its control goal if it is unstable. Typically, the majority of the control stability can be analyzed and proved by linear analysis techniques (Sastry and Bodson, 2011). However, the receding horizon MPC control with constraints, such as the MPC- q_0 , MPC- q_1 and MPC- q_2 in this study constitute a nonlinear feedback control system, of which the standard linear techniques are insufficient to prove the stability. To tackle this challenge, we employ the Lyapunov theory in Theorem 1 below to characterize the nominal system² behaviors and prove the asymptotical stability of the nominal MPC- q_0 first.

Theorem 1. Asymptotic Stability (Bof et al., 2018): Let $\varphi = 0$ be an equilibrium point for the autonomous system $\varphi(k+1) = f(\varphi(k))$, where $f: D \to \mathbb{R}^n$ is locally Lipschitz in $D \subset \mathbb{R}^n$ and $0 \in D$. Suppose there exists a function $V: D \to \mathbb{R}^n$ which is continuous and such that (i) V ($\varphi = 0$) = 0 and $V(\varphi) > 0$ for $\forall \varphi \in D - \{0\}$; (ii) $V(f(\varphi(k))) - V(\varphi) \le 0$ for $\forall \varphi \in D$, then $\varphi = 0$ is stable. The function V that satisfies conditions (i) and (ii) is called Lyapunov function. Moreover, if (iii) $V(f(\varphi(k))) - V(\varphi) < 0$ for $\forall \varphi \in D - \{0\}$, then $\varphi = 0$ is asymptotic stable.

Furthermore, this study is aware that the uncertainties in Eq. (4) makes our MPC- q_0 a robust system rather than the nominal system. Proving the stability of the nominal system is not sufficient for this study. We therefore continue to prove the Input-to-State stability of MPC- q_0 in **Remark 1** based upon Theorem 2. The Input-to-State stability ensures the system states are bounded around the equilibrium point (i.e., the steady-state of the platoon), when uncertainties are involved. In other words, the platoon under the MPC- q_0 control in this study will perform well under control uncertainties, if it is Input-to-State stable.

Theorem 2. Input-to-State Stability (Zeilinger et al., 2009): The discrete-time robust linear system $\varphi(k+1) = A\varphi(k) + Bu(k) + w(k)$ is Input-to-State stable if the corresponding nominal system $\varphi(k+1) = A\varphi(k) + Bu(k)$ is asymptotically stable and the disturbance w(k) is bounded.

Please note that the stability (e.g., Input-to-State stability) is used to evaluate the performance of an MPC in the long term. MPC- q_1 and MPC- q_2 are the controllers with shrinking prediction horizons. They are only used for a short time period when the platoon is near the intersection. Hence, we only show the stability proof for MPC- q_0 .

5.1. Reformulation and nominal system of the MPC-q₀

Before developing our stability analyses, we first rewrite Eqs. (2)-(4) and (9)-(13) into Eqs. (38) and (39) respectively,

$$\varphi(k+1) = A\varphi(k) + Bu(k) + w(k) \tag{38}$$

$$\varphi(k+1) = A\varphi(k) + Bu(k) \tag{39}$$

where for $\forall k \in \mathbb{Z}_+$, $\varphi(k) = \begin{bmatrix} z(k) \\ z'(k) \end{bmatrix} \in \mathbb{R}^{2N}$ is the control state, $u(k) \in \mathbb{R}^{N+1}$ is the control input, $w(k) \in W \in \mathbb{R}^{2N}$ is the bounded uncertainty that is contained in a convex and compact set introduced by Eq. (4). Eq. (38) is discrete-time robust control dynamics of our MPC- q_0 , whereas Eq. (39) is the corresponding nominal control dynamics by taking off the uncertainty w(k). Then, we have A, B and W defined in Eq. (40). The corresponding mathematical derivations to obtain them are provided in the Appendix A1.

$$A = \begin{bmatrix} I_N & \tau I_N \\ 0 & I_N \end{bmatrix} \in \mathbb{R}^{2N \times 2N}; B = \begin{bmatrix} \tau^2 S_1 \\ \tau S_2 \end{bmatrix} \in \mathbb{R}^{2N \times (N+1)}; W = \begin{bmatrix} -\begin{bmatrix} \tau^2 S_1 \\ \tau S_2 \end{bmatrix} \overline{\Delta}_i, -\begin{bmatrix} \tau^2 S_1 \\ \tau S_2 \end{bmatrix} \underline{\Delta}_i \end{bmatrix}$$

$$(40)$$

The matrix S_1, S_2 in Eq. (40) are shown below, where $c_1 = \delta_2 + \frac{1}{2}$; $c_2 = -(\delta_1 + \delta_2 + \frac{1}{2})$:

$$S_1 = \begin{bmatrix} c_1 & c_2 & & & \\ & c_1 & c_2 & & \\ & & \ddots & \ddots & \\ & & & c_1 & c_2 \end{bmatrix} \in \mathbb{R}^{N \times \ (N+1)}; \ S_2 = \begin{bmatrix} 1 & -1 & & & \\ & 1 & -1 & & \\ & & \ddots & \ddots & \\ & & & 1 & -1 \end{bmatrix} \in \mathbb{R}^{N \times \ (N+1)}.$$

Next, we transform the robust MPC- q_0 developed in Section 3 into the nominal system MPC- \mathbb{Q}_0 below using the nominal control dynamics in Eq. (39). Note that the CAV control uncertainty in Eq. (4) is removed.

$$MPC - \mathbb{Q}_0 \min_{u} \Gamma(k) = \sum_{p=1}^{p} \mathscr{N}(\varphi(p|k), u(p|k))$$

Subject to: $\varphi(p + 1|k) = A\varphi(p|k) + Bu(p|k), p = 0, 1, ..., P - 1$

² Nominal system is defined as the system's dynamics without modeling uncertainty errors

$$(\varphi(p+1|k), u(p|k)) \in \Phi \times U, p=0, 1, ..., P-1$$

 $\varphi(P|k) \in \Phi_r$

The notation (p|k) in the MPC- \mathbb{Q}_0 represents the time step of p+k; Φ and U are linear constraints on the states and inputs corresponding to Eqs. (5)–(8). According to the MPC- q_0 objective function in Eq. (1), the stage cost is defined as $\mathscr{L}(\varphi(p|k), \mu(p|k)) := \frac{1}{2}[z^T(p|k)Q_zz(p|k) + (z^{'}(p|k))^TQ_z^{'}z^{'}(p|k)] + \frac{r^2}{2}\omega_1\|u(p-1|k)\|_2^2$. Φ_f is the compact terminal constraint defined in Eq. (39). Please note that under the nominal system in the Eq. (39), Φ_f becomes the equilibrium point, namely $\Phi_f = 0$: z(P|k) = 0, z'(P|k) = 0.

Solving the MPC- \mathbb{Q}_0 will generate an optimal control sequence $\widehat{u}(k) = [u^*(0|k), u(1|k), ..., u(P-1|k)]$, in which the MPC controller will only implement the current control decision $u^*(0|k)$, and recompute MPC- \mathbb{Q}_0 at the next time step. $u^*(0|k)$ can be considered as a feedback control of the current state $\varphi(0|k)$ at step k as follows in Eq. (41):

$$u^*(0|k) = K_f \varphi(0|k)$$
 (41)

where K_f is the corresponding feedback control law obtained by solving MPG- \mathbb{Q}_0 . From the optimal control sequence $\widehat{u}(k)$, we can obtain corresponding state sequence $\widehat{\varphi}(k) = [\varphi(1|k), \varphi(2|k), ..., \varphi(P|k)]$ as well as the optimal value function $\Gamma_V(k, \widehat{u}(k))$ of the MPG- \mathbb{Q}_0 . $\Gamma_V(k, \widehat{u}(k))$ is the value of the objective function $\Gamma(k)$ when the optimal control sequence $\widehat{u}(k)$ is applied to the system. The value function $\Gamma_V(k, \widehat{u}(k))$ will be employed as a Lyapunov function to prove the asymptotic stability in the next Section 5.2. We abbreviate $\Gamma_V(k, \widehat{u}(k))$ as $\Gamma_V(k)$ hereafter for discussion convenience.

5.2. Asymptotic Stability and Input-to-State Stability

This section proves the asymptotical stability of the nominal MPC- \mathbb{Q}_0 and then the Input-to-State stability of the robust MPC- q_0 . Specifically, we first show $\Gamma_V(k)$ is a Lyapunov function and thus the nominal MPC- \mathbb{Q}_0 is asymptotic stable in Lemma 2 according to the Lyapunov Theory in Theorem 1. Then together Theorem 2, we conclude the robust MPC- q_0 is Input-to-State stable in Remark 1.

Lemma 2. Suppose $\Gamma_V(k)$ is the optimal value function of MPC- \mathbb{Q}_0 , then $\Gamma_V(k)$ is a Lyapunov function and MPC- \mathbb{Q}_0 is asymptotic stable.

Proof. According to the feedback control law in Eq. (41), the nominal controller in Eq. (39) can be converted into $\varphi(k+1) = (A+BK_f)\varphi(k)$ for $\forall k \in \mathbb{Z}_+$, which is an autonomous system stated in Theorem 1. Accordingly, the autonomous system dynamic function $f = A+BK_f$ is linear time invariant and thus Lipschitz in a domain $D=\mathbb{R}^N$. Then, to prove $\Gamma_V(k)$ is a Lyapunov function and MPC- \mathbb{Q}_0 is asymptotic stable, we need to prove the function $\Gamma_V(k)$ satisfies the three conditions in Theorem 1, which are (i) $\Gamma_V(\varphi(k) = 0) = 0$ and $\Gamma_V(\varphi(k)) > 0$ for $\forall \varphi(k) \in \mathbb{R}^N - \{0\}$; (iii) $\Gamma_V(f(\varphi(k))) - \Gamma_V(\varphi(k)) \leq 0$ for $\forall \varphi(k) \in \mathbb{R}^N$; (iii) $\Gamma_V(f(\varphi(k))) - \Gamma_V(\varphi(k)) \leq 0$ for $\forall \varphi(k) \in \mathbb{R}^N$.

Recall that $\Gamma_V(k)$ represents the optimal value of the objective function $\Gamma(k)$ in the MPC- \mathbb{Q}_0 , which is obtained by applying the optimal control sequence $\widehat{u}(k)$ to the system³. The quadratic formulation of $\Gamma(k)$ in Eq. (1) indicates $\Gamma(k) \geq 0$ so that we have $\Gamma_V(k) \geq 0$. Apart from it, $\Gamma_V(k) = 0$ holds if and only if the MPC- \mathbb{Q}_0 reaches equilibrium point (i.e., $\varphi(k) = 0$, all CAV keep same reference speed and apart with desired spacing). Hence, condition (i) is satisfied.

Then, we need to show conditions (ii) and (iii) are satisfied. Specifically, $\Gamma_V(k+1) < \Gamma_V(k)$ for $\forall \varphi \in \mathbb{R}^N - \{0\}$ and $\Gamma_V(k+1) = \Gamma_V(k)$ when $\varphi = 0$. The mathematical definition of function $\Gamma_V(k)$ and $\Gamma_V(k+1)$ are given below in Eqs. (42) and (43).

$$\Gamma_{V}(k) = \min_{u} \sum_{n=1}^{P} \mathscr{N}(\varphi(p|k), u(p-1|k)) = \min_{u} \sum_{n=1}^{P} \mathscr{N}(\varphi(p+k), u(p+k-1))$$
 (42)

$$\Gamma_{V}(k+1) = \min_{u} \sum_{p=1}^{P} \mathcal{L}(\varphi(p+k+1), u(p+k))$$
 (43)

According to Eqs. (42) and (43), we have the following mathematical derivations for $\Gamma_V(k+1)$ in Eq. (44).

$$\Gamma_{V}(k+1) = \min_{u} \left\{ \sum_{p=1}^{P-1} \ell(\varphi(p+k+1), u(p+k)) + \ell(\varphi(P+k+1), u(P+k)) \right\}$$

$$= \min_{u} \left\{ \sum_{p=2}^{P} \ell(\varphi(p+k), u(p+k-1)) + \ell(\varphi(k+1), u(k)) \right\} - \min_{u(k)} \ell(\varphi(k+1), u(k)) + \min_{u(P+k)} \ell(\varphi(P+k+1), u(P+k))$$

$$= \Gamma_{V}(k) - \min_{u(k)} \ell(\varphi(k+1), u(k)) + \min_{u(P+k)} \ell(\varphi(P+k+1), u(P+k))$$
(44)

Since we define the terminal constraint $\varphi(P|k) \in \Phi_f = 0$ in the nominal MPC- \mathbb{Q}_0 , we have the state φ reach the equilibrium point at step k + P (i.e., $\varphi(P + k) = 0$). Then there exits feasible control input u(P + k) = 0 to drive the state φ stay at the equilibrium point 0,

 $^{^3}$ $\Gamma_V(k)$ refers to $\Gamma_V(\varphi(k))$ and correspondingly $\Gamma_V(k+1)$ refers to $\Gamma_V(f(\varphi(k)))$.

H. Zhang and L. Du

namely $\varphi(P+k+1)=0$. Hence, $\min_{u(P+k)} \ell(\varphi(P+k+1),u(P+k))=0$. Together Eq. (44), we have the following Eq. (45).

$$\Gamma_V(k+1) \le \Gamma_V(k) - \min_{u(k)} (\varphi(k+1), u(k)) \tag{45}$$

Further, based on Eq. (45) and $\ell(\varphi(k+1), u(k)) \ge 0$, we have

$$\Gamma_V(k+1) < \Gamma_V(k)$$

Condition (ii) is satisfied. Moreover $\Gamma_V(k+1) = \Gamma_V(k)$ holds if and only if $\ell(\varphi(k+1), u(k)) = 0$, namely $\varphi(k) = 0$, u(k) = 0. Condition (iii) is satisfied. In summary, function $\Gamma_V(k)$ is a Lyapunov function that satisfies three conditions in Theorem 1. Hence, MPC- \mathbb{Q}_0 is asymptotic stable. We conclude the proof.

Remark 1. Given that the uncertainty w(k) is bounded and Lemma 2 has proved that the nominal MPC- \mathbb{Q}_0 is asymptotic stable, we claim that the robust MPC- q_0 is Input-to-State stable according to Theorem 2. It ensures that the platoon states such as vehicle speeds and spacings in this study are bounded around our desired control goal under the robust MPC control. Besides, the gap between the actual control performance and our literal control goal highly depends on the uncertainty w(k). Specifically, the gap decreases as the uncertainty w(k) becomes smaller. When w(k) = 0, the system becomes nominal system without uncertainty and the gap becomes 0.

Remark 2. Although this study does not explicitly model the impact of CAV communication delay in the MPC- q_0 , the bounded CAV communication delay will not affect the stability of the MPC- q_0 . Specifically, the negative impacts caused by the bounded communication delay can be factored into the bounded control uncertainties w(k) in CAV's robust dynamic system through Eq. (38). Given the communication delay is bounded, the resulting control uncertainty w(k) will also be bounded. Then the MPC- q_0 is still Input-to-State stable according to **Remark 1**. On the other hand, if the communication lag is large and unbounded (e.g., communication fails), MPC feasibility and system stability are hard to be ensured. One possible solution for addressing this challenge is to use a machine learning approach to detect such anomalies and exclude such CAVs with significant communication lags using finite state machine in platoon according to Smith et al., (2020). As in this case, the CAVs with significant communication lags are not well connected, from which the platoon is separated into two individual platoons. However, this topic is out of the scope of the research in this paper. We propose to do it in our future work.

6. Theoretical analysis of the AS-OCD

Part I of this study developed an active-set-based optimal condition decomposition approach (AS-OCD) to solve the MPC optimizers of the hybrid system via a distributed optimization approach. The numerical experiments have validated its effectiveness in practice. This section in Part II focuses on analyzing its theoretical performance, including solution optimality and convergence speed.

6.1. Active set based optimal condition decomposition (AS-OCD)

For completeness, we first briefly review the key ideas and formulations of the AS-OCD algorithm to provide the mathematical foundation for our theoretical analysis. Please refer to the Part I paper (Zhang and Du, 2022) for the technical details. The AS-OCD algorithm combines the active set method (AS) (Nocedal and Wright, 2006; Nak et al., 2017) and the optimal condition decomposition approach (OCD) (Conejo et al., 2002). Mainly, the AS algorithm identifies the violated constraints by the current solution of the MPC controllers and then makes them become active constraints. This procedure renders the following Optimizer F in Eq. (46), which is rewritten from MPC- q_0 but only subject to equality constraints. Next, the OCD algorithm is used to solve optimizer F in distributed computing fashion. The two procedures are iteratively conducted until AS cannot find the violated inactive constraints.

Optimizer
$$F: \text{ Min } \Gamma(u) = \sum_{i=1}^{N} \left\{ z_{i}^{T} Q_{z_{i}} z_{i} + \left(z_{i}^{'} \right)^{T} Q_{z_{i}^{'}} z_{i}^{'} + \frac{\tau^{2}}{2} \| u_{i} \|_{2}^{2} \right\}$$
 (46)

Subject to *l*-many $g_{AS}(u_{i-1}, u_i) = 0$, ℓ -many $c_{AS}(u_{i}) = 0$,

In the optimizer F in Eq. (46), $g_{AS}(u_{j-1}, u_{j}) = 0$ is an active coupled constraint such as safe distance constraints in Eq. (8) while constraint $c_{AS}(u_{j}) = 0$ is active uncoupled constraints such as acceleration/speed limits in Eqs. (6)–(7).

Clearly, the OCD algorithm is critical to ensuring convergence and computation efficiency. We provide more technical details in this regard. The Karush–Kuhn–Tucker (KKT) conditions (Boyd et al., 2004) of the convex optimizer *F* lead to a system of equations. Newton's method (Nocedal and Wright, 2006) in Eq. (47) is an efficient approach to find the global optimal solution for such system.

⁴ Given an optimization problem, an inequality constraint $g(x) \ge 0$ is called active at x if g(x) = 0 and inactive at x if g(x) > 0, whereas equality constraints are always active.

⁵ Coupled constraints refer to the constraints involving more than two agents (two CAVs in this study). Conversely, uncoupled constraints involve only one agent (one CAV).

H. Zhang and L. Du

$$\begin{array}{cccc}
\nabla^{2}L_{AS}(u,\eta,\lambda) & \nabla^{T}C_{AS}(u) & \nabla^{T}g_{AS}(u) & \Delta u \\
\nabla^{2}C_{AS}(u) & 0 & 0 & C_{AS}(u) \\
\nabla^{2}G_{AS}(u) & 0 & 0 & C_{AS}(u)
\end{array}$$

$$\Rightarrow K\Delta = -f$$
(47)

where $L_{AS}(u,\eta,\lambda) = \Gamma(u) + \eta^T c_{AS}(u) + \lambda^T g_{AS}(u)$ is the Lagrangian function derived from Optimizer F; $\eta = [\eta_1,...,\eta_{\ell}]^T$ and $\lambda = [\lambda_1,...,\lambda_l]^T$ are Lagrange multipliers; the searching direction Δ is obtained by solving $\Delta = -K^{-1}f$ and then is used to update the solution iteratively until converging to the optimal solution.

This Newton's method needs to be implemented by a central solver since the KKT matrix K involves coupled elements: $\nabla^2 L_{AS}(u,\eta,\lambda)$, $\nabla g_{AS}(u)$. For example, $\nabla^2 L_{AS}(u,\eta,\lambda)$ is related to the objective function $\Gamma(u)$ in Eq. (1) where the neighboring CAVs' control inputs are closely coupled in terms of the platoon control dynamics in Eqs. (9)–(13)). $\nabla g_{AS}(u)$ is the gradient of safe distance constraints in Eq. (8) and thus also couples two neighboring CAVs' states. However, our experiments found that centralized computation cannot provide satisfying performance for this real-time control. Part I of this study thus explored the OCD algorithm. A critical modification is to approximate the KKT matrix K in Eq. (47) to \overline{K} in Eq. (48).

$$\underbrace{\begin{pmatrix} \overline{K}_1 & 0 & 0 \\ 0 & \ddots & 0 \\ 0 & 0 & \overline{K}_N \end{pmatrix}}_{\overline{K}} \underbrace{\begin{pmatrix} \overline{\Delta}_1 \\ \vdots \\ \overline{\Delta}_N \end{pmatrix}}_{\overline{\Lambda}} = -\underbrace{\begin{pmatrix} f_1 \\ \vdots \\ f_N \end{pmatrix}}_{\overline{I}} \Leftrightarrow \overline{\Delta}_1 = -\overline{K}_i^{-1} f_i, \ \forall i = 1, ..., N, \tag{48}$$

where \overline{K}_i is the matrix block of CAV i in the approximated KKT matrix \overline{K} ; $\overline{\Delta}_i$ and f_i represent CAV i's searching direction and corresponding gradient. The mathematical formulations of \overline{K}_i , $\overline{\Delta}_i$, f_i are given in Appendix A2. Apparently, CAVs' control variables in \overline{K} are separable. Accordingly, we can compute each CAV i's searching direction by $\overline{\Delta}_i = -\overline{K}_i^{-1}f_i$ in a distributed manner. To be noted, this approximation of the KKT matrix will not affect the solution optimality and the convergence of the OCD algorithm. We will demonstrate these technical details in section 6.2.

6.2. Convergence of the AS-OCD

This AS-OCD algorithm is an iterative distributed algorithm. Then, it posed the theoretical questions regarding its convergence performance (i.e., whether the AS-OCD can converge to the optimal solution and how fast it converges). We investigate these issues in this section. The main idea is given as follows. According to the study of Nocedal and Wright, (2006), the AS method can converge to the global optimal solution for a strictly convex quadratic problem with linear constraints. It works efficiently for optimization problems with few active constraints. The MPC optimizers of this study satisfy these features. Hence, the convergence rate and solution optimality of the AS-OCD algorithm highly depends on the performance of the OCD algorithm. According to Theorem 3 in Conejo et al., (2002), the OCD algorithm can guarantee the linear convergence rate to the global optimal solution when an optimizer satisfies certain conditions. We will use this Theorem 3 to prove the convergence of the OCD algorithm. For completeness, we provide Theorem 3 first as follows.

Theorem 3. (Conejo et al., 2002) For an optimizer F in Eq. (46), using the OCD algorithm can obtain the global optimal solution l^* with linear convergence rate at least equal to l^* if the following conditions hold.

- (I) Functions Γ , g, c have Lipschitz-continuous second derivatives in an open set containing l^* ;
- (II) The matrix \overline{K} is nonsingular for any l, and the sequence $\{\overline{K}\}$ converges to a nonsingular matrix \overline{K} as $l \to l^*$;
- (III) At the second order KKT point l^* , $\rho^* = \rho(I (\overline{K})^{-1}K) < 1$.

Built upon Theorem 3, we prove Lemma 3 to confirm that the OCD algorithm can obtain global optimal solutions efficiently.

Lemma 3. The MPC optimizer F in Eq. (46) satisfies conditions (I), (II) and (III) in Theorem 3 and thus can obtain global optimal solution in linear convergence rate using OCD algorithm.

Proof: First of all, the functions Γ , g and c of the MPC optimizer F in Eq. (46) are quadratic or linear. Then they are globally second-order Lipschitz-continuous according to Sohrab, (2003). Thus, Condition (I) is satisfied. Next, given that the matrix \overline{K} is the hessian matrix of Γ when constraints g, c are not active, then \overline{K} is constant because Γ is quadratic. Besides, \overline{K} is diagonalizable and we can easily show Γ is strictly convex with positive eigenvalues according to Eq. (46) and MPC- q_0 optimizer in Eq. (1). Hence, \overline{K} has full rank and is always nonsingular (Greub, 2012). Condition (II) is satisfied.

Then, we focus on proving condition (III) holds by showing the spectral radius (all the eigenvalues) of the matrix $(I - (\overline{K})^{-1}K)$ is smaller than 1 (i.e., $\rho^* < 1$). To do that, we first provide the explicit expression of the matrix $(I - (\overline{K})^{-1}K)$. Then we use the induced

⁶ The global optimal solution $l^* = (u^*, \sigma^*, \lambda^*)$ is the second-order KKT point of optimizer *F*. When optimizer *F* is convex, l^* is the optimal solution.

⁷ Nonsingular matrix is a square matrix whose determinant is not equal to zero (i.e., has full rank).

 $^{^8}$ If a matrix A is Hermitian symmetric, then A is diagonalizable. \overline{K} is symmetric and thus diagonalizable.

norm inequality $\rho(A) \leq \|A\|$ to prove the spectral radius of matrix $(I - (\overline{K})^{-1}K)$ is less than 1. The proof details are given as follows. To prove condition (iii) $\rho^* = \rho(I - (\overline{K})^{-1}K) < 1$ holds, we first write the mathematical formulations of the matrices K and \overline{K} in Eq. (49). Note that the objective function $\Gamma(u)$ in Eq. (46) is locally coupled, namely CAV i's control input u_i is only coupled with two control inputs u_{i-1} , u_{i+1} of its immediate neighboring CAVs. According to this feature, we have $\frac{\partial^2 \Gamma}{\partial u u} = 0$ if $|i-j| \geq 2$.

$$K = \begin{bmatrix} \frac{\partial^{2} \Gamma}{\partial u_{1}^{2}} & \frac{\partial^{2} \Gamma}{\partial u_{1} u_{2}} & 0 & \dots & 0 \\ \frac{\partial^{2} \Gamma}{\partial u_{2} u_{1}} & \frac{\partial^{2} \Gamma}{\partial u_{2}^{2}} & \frac{\partial^{2} \Gamma}{\partial u_{2} u_{3}} & \ddots & \vdots \\ 0 & \frac{\partial^{2} \Gamma}{\partial u_{3} u_{2}} & \ddots & \ddots & 0 \\ \vdots & \ddots & \ddots & \frac{\partial^{2} \Gamma}{\partial u_{N-1}^{2}} & \frac{\partial^{2} \Gamma}{\partial u_{N-1} u_{N}} \end{bmatrix} \overline{K} = \begin{bmatrix} \frac{\partial^{2} \Gamma}{\partial u_{1}^{2}} & 0 & 0 & \dots & 0 \\ 0 & \frac{\partial^{2} \Gamma}{\partial u_{2}^{2}} & 0 & \ddots & \vdots \\ 0 & \ddots & \ddots & \ddots & 0 \\ \vdots & \ddots & 0 & \frac{\partial^{2} \Gamma}{\partial u_{N-1}^{2}} & 0 \\ \vdots & \ddots & 0 & \frac{\partial^{2} \Gamma}{\partial u_{N-1}^{2}} & 0 \end{bmatrix}.$$

$$(49)$$

It is noted that matrices K and \overline{K} in Eq. (49) do not consider the constraints in Eqs. (6)–(8) and (14) because they are not active under normal traffic conditions. Besides, involving these constraints will introduce Lagrangian multipliers η and λ into the Lagrangian function L_{AS} in Eqs. (47). Given multipliers η and λ can be any negative or positive value, the matrices K and \overline{K} in Eqs. (47)–(48) are hard to bound. Consequently, theoretically proving condition (iii) becomes mathematically intractable according to Conejo et al. (2002).

According to Eq. (49), we can sequentially derive the matrix $(\overline{K})^{-1}K$ in Eq. (50) and finally the matrix $I - (\overline{K})^{-1}K$ in Eq. (51) below.

$$(\overline{K})^{-1}K = \begin{bmatrix} I_P & A_{1,2} & 0 & \dots & 0 \\ A_{2,1} & I_P & A_{2,3} & \ddots & \vdots \\ 0 & A_{3,2} & \ddots & \ddots & 0 \\ \vdots & \ddots & \ddots & I_P & A_{N-1,N} \\ 0 & \dots & 0 & A_{NN-1} & I_P \end{bmatrix},$$
(50)

$$B = \begin{bmatrix} B_1 \\ B_2 \\ \vdots \\ B_{N-1} \\ B_N \end{bmatrix} = I - (\overline{K})^{-1} K = \begin{bmatrix} 0 & -A_{1,2} & 0 & \dots & 0 \\ -A_{2,1} & 0 & -A_{2,3} & \ddots & \vdots \\ 0 & -A_{3,2} & \ddots & \ddots & 0 \\ \vdots & \ddots & \ddots & 0 & -A_{N-1,N} \\ 0 & \dots & 0 & -A_{N,N-1} & 0 \end{bmatrix},$$
(51)

Note that we use $B = I - (\overline{K})^{-1}K$ hereafter for discussion convenience. To prove condition (III) holds, it is equivalent to showing the spectral radius of matrix B is less than 1. We intend to use the induced norm inequality to prove it. Specifically, we first calculate the 1-norm of matrix B (i.e, $\|B\|$) and show $\|B\|$ is less than 1. It is equivalent to showing the summation of the row elements' absolute values is less than 1 for every row of matrix B. For discussion convenience, we denote $B = \begin{bmatrix} B_1 & B_2 & \dots & B_{N-1} & B_N \end{bmatrix}^T$, where $B_i \in \mathbb{R}^{P \times NP}$ represents i^{th} row block of matrix B with P rows. B_i corresponds to CAV i's P-step matrix block in the optimizer $\Gamma(u)$. Further, we use the notation $B_{i,p}$ to represent the p^{th} row of the matrix block B_i , $\forall p = 1, \dots, P$, $B_{i,p}$ corresponds to CAV i's matrix block at time step P. Wrapping above, if the 1-norm of $B_{i,p}$ (i.e., $\|B_{i,p}\|$) is less than 1 for $\forall i = 1, \dots, N, \forall p = 1, \dots, P$, condition (III) holds. Below we show $\|B_{i,p}\|$ is always less than 1.

To do that, we first have $B_i, \forall i = 1, ..., N$ represented as follows in Eq. (52).

$$B_{i} = \begin{cases} -A_{i,i+1} = -\left(\frac{\partial^{2}\Gamma}{\partial u_{i}^{2}}\right)^{-1} \frac{\partial^{2}\Gamma}{\partial u_{i}u_{i+1}} & \text{if } i = 1\\ -A_{i,i-1} - A_{i,i+1} = -\left(\frac{\partial^{2}\Gamma}{\partial u_{i}^{2}}\right)^{-1} \left(\frac{\partial^{2}\Gamma}{\partial u_{i}u_{i-1}} + \frac{\partial^{2}\Gamma}{\partial u_{i}u_{i+1}}\right) & \text{if } i \neq 1, N \end{cases}$$

$$-A_{i,i-1} = -\left(\frac{\partial^{2}\Gamma}{\partial u_{i}^{2}}\right)^{-1} \frac{\partial^{2}\Gamma}{\partial u_{i}u_{i-1}} & \text{if } i = N \end{cases}$$
(52)

⁹ For a matrix A, $\rho(A) \le \|A^r Apt Command 2016;^{1/r}$ for all positive integers r, where $\rho(A)$ is the spectral radius of A. When = 1, $\rho(A) \le \|A\|$, $\|A\|$ is the 1-norm of matrix A.

¹⁰ sely, uncoupled constraints involve only one agent (one CAV).

According to Eq. (52), we can obtain $||B_{i,p}||$ in Eq. (53) for each row $p_1 \in \{1, ..., P\}$ in B_{i} .

$$\|B_{i,p}\| = \begin{cases} \sum_{p_{2}=1}^{P} \left| \frac{\partial^{2}\Gamma}{\partial u_{i}(p_{1})u_{i}(p_{2})} \right|^{-1} \left| \frac{\partial^{2}\Gamma}{\partial u_{i}(p_{1})u_{i+1}(p_{2})} \right| & i = 1 \\ \sum_{p_{2}=1}^{P} \left| \frac{\partial^{2}\Gamma}{\partial u_{i}(p_{1})u_{i}(p_{2})} \right|^{-1} \left| \frac{\partial^{2}\Gamma}{\partial u_{i}(p_{1})u_{i-1}(p_{2})} + \frac{\partial^{2}\Gamma}{\partial u_{i}(p_{1})u_{i+1}(p_{2})} \right| & i \neq 1, N \end{cases}$$

$$\sum_{p_{2}=1}^{P} \left| \frac{\partial^{2}\Gamma}{\partial u_{i}(p_{1})u_{i}(p_{2})} \right|^{-1} \left| \frac{\partial^{2}\Gamma}{\partial u_{i}(p_{1})u_{i-1}(p_{2})} \right| & i = N \end{cases}$$
(53)

Consequently, to prove $||B_{i,p}|| < 1$, we need to derive out the mathematical representation of $\frac{\partial^2 \Gamma}{\partial u_i(p_1)u_i(p_2)}$, $\frac{\partial^2 \Gamma}{\partial u_i(p_1)u_{i-1}(p_2)}$, $\frac{\partial^2 \Gamma}{\partial u_i(p_1)u_{i-1}(p_2)}$ and show each element of $||B_{i,p}||$ is strictly less than 1. To do that, we calculate the second derivatives $\frac{\partial^2 \Gamma}{\partial u_i(p_1)u_i(p_2)}$, $\frac{\partial^2 \Gamma}{\partial u_i(p_1)u_{i-1}(p_2)}$ and $\frac{\partial^2 \Gamma}{\partial u_i(p_1)u_{i-1}(p_2)}$ and $\frac{\partial^2 \Gamma}{\partial u_i(p_1)u_{i-1}(p_2)}$ and $\frac{\partial^2 \Gamma}{\partial u_i(p_1)u_{i-1}(p_2)}$

$$\frac{\partial^2 \Gamma}{\partial u_i(p_1)u_i(p_2)} = \sum_{p=\max\{p_1,p_2\}}^{P} \left[\alpha_i \frac{\partial z_i(p)}{\partial u_i(p_1)} \frac{\partial z_i(p)}{\partial u_i(p_2)} + \beta_i \frac{\partial z_i'(p)}{\partial u_i(p_2)} \frac{\partial z_i'(p)}{\partial u_i(p_2)} + \alpha_{i+1} \frac{\partial z_{i+1}(p)}{\partial u_i(p_1)} \frac{\partial z_{i+1}(p)}{\partial u_i(p_2)} + \beta_{i+1} \frac{\partial z_{i+1}'(p)}{\partial u_i(p_2)} \frac{\partial z_{i+1}'(p)}{\partial u_i(p_2)} + \alpha_{1} \frac{\partial z_{i+1}'(p)}{\partial u_i(p_2)} \frac{\partial z_{i+1}'(p)}{\partial u_i(p_2)} \frac{\partial z_{i+1}'(p)}{\partial u_i(p_2)} + \alpha_{1} \frac{\partial z_{i+1}'(p)}{\partial u_i(p_2)} \frac{\partial z_{i+1}'(p)}{\partial u_i(p_2)} \frac{\partial z_{i+1}'(p)}{\partial u_i(p_2)} + \alpha_{1} \frac{\partial z_{i+1}'(p)}{\partial u_i(p_2)} \frac{\partial z_{i+1}'(p)}{\partial u_i(p_2)$$

$$\frac{\partial^{2}\Gamma}{\partial u_{i}(p_{1})u_{i-1}(p_{2})} = \sum_{p=\max\{p_{1},p_{2}\}}^{P} \left[\alpha_{i} \frac{\partial z_{i}(p)}{\partial u_{i}(p_{1})} \frac{\partial z_{i}(p)}{\partial u_{i-1}(p_{2})} + \beta_{i} \frac{\partial z_{i}'(p)}{\partial u_{i}(p_{1})} \frac{\partial z_{i}'(p)}{\partial u_{i-1}(p_{2})} \right], \tag{55}$$

$$\frac{\partial^{2} \Gamma}{\partial u_{i}(p_{1}) u_{i+1}(p_{2})} = \sum_{p=\max\{p_{1},p_{2}\}}^{P} \left[\alpha_{i+1} \frac{\partial z_{i+1}(p)}{\partial u_{i}(p_{1})} \frac{\partial z_{i+1}(p)}{\partial u_{i+1}(p_{2})} + \beta_{i+1} \frac{\partial z_{i+1}^{'}(p)}{\partial u_{i}(p_{1})} \frac{\partial z_{i+1}^{'}(p)}{\partial u_{i+1}(p_{2})} \right], \tag{56}$$

In Eq. (54), $\zeta(p_1,p_2) = \{ \begin{array}{l} 1 \text{ if } p_1 = p_2 \\ 0 \text{ otherwise} \end{array} \text{ is an indicator function. In Eqs. (54)–(56), the first derivative } \frac{\partial z_i(p)}{\partial u_{i-1}(p_2)}, \frac{\partial z_{i+1}(p)}{\partial u_i(p_2)}, \frac{\partial z_{i+1}(p)}{\partial u_{i+1}(p_2)} \text{ and } \frac{\partial z_{i+1}'(p)}{\partial u_i(p_2)} \\ \text{are formulated below in Eq. (57) according to Eqs. (9)–(13).} \end{array}$

$$\frac{\partial z_{i}(p)}{\partial u_{i-1}(p_{2})} = \frac{\partial x_{i-1}(p)}{\partial u_{i-1}(p_{2})} + \delta_{2}\tau \frac{\partial v_{i-1}(p)}{\partial u_{i-1}(p_{2})}; \quad \frac{\partial z_{i+1}^{'}(p)}{\partial u_{i}(p_{2})} = \frac{\partial v_{i}(p)}{\partial u_{i}(p_{2})}$$

$$\frac{\partial z_i(p)}{\partial u_i(p_2)} = -\frac{\partial x_i(p)}{\partial u_i(p_2)} - (\delta_1 + \delta_2)\tau \frac{\partial v_i(p)}{\partial u_i(p_2)}; \quad \frac{\partial z'_{i+1}(p)}{\partial u_{i+1}(p_2)} = -\frac{\partial v_{i+1}(p)}{\partial u_{i+1}(p_2)}$$

$$(57)$$

Without loss of generality, we consider CAVs' aerodynamic drag and powertrain lag coefficients are the same for discussion convenience so that we can have $|\frac{\partial v_l(p)}{\partial u_l(p_2)}| = |\frac{\partial v_{l+1}(p)}{\partial u_{l+1}(p_2)}|$ and $|\frac{\partial x_{l-1}(p)}{\partial u_{l-1}(p_2)}| = |\frac{\partial x_{l+1}(p)}{\partial u_l(p_2)}|$ according to Eqs. (2)–(4). Then we have the following relations regarding $\frac{\partial z_i(p)}{\partial u_l(p_2)}$, $\frac{\partial z_i(p)}{\partial u_l(p_2)}$, $\frac{\partial z_i(p)}{\partial u_l(p_2)}$, $\frac{\partial z_i(p)}{\partial u_l(p_2)}$ and $\frac{\partial z_{i+1}(p)}{\partial u_l(p_2)}$ in Eq. (58) based on Eq. (57). Note that if CAVs' aerodynamic drag and powertrain lag are different, $|\frac{\partial v_l(p)}{\partial u_l(p_2)}|$ and $|\frac{\partial x_l(p)}{\partial u_l(p_2)}|$ may be smaller or larger than $|\frac{\partial v_{l+1}(p)}{\partial u_{l+1}(p_2)}|$ and $|\frac{\partial x_{l+1}(p)}{\partial u_{l-1}(p_2)}|$ respectively. It will make the math relations in Eqs. (58)–(59) very complicated with a large number of scenarios, and consequently lead to Eq. (53) mathematically intractable. Besides, CAVs' aerodynamic drag and powertrain lag are normally small, so it is reasonable to consider them the same values without affecting the final results.

$$\left| \frac{\partial z'_{i+1}(p)}{\partial u_{i+1}(p_2)} \right| = \left| \frac{\partial z'_{i+1}(p)}{\partial u_i(p_2)} \right|; \quad \left| \frac{\partial z_i(p)}{\partial u_{i-1}(p_2)} \right| < \left| \frac{\partial z_i(p)}{\partial u_i(p_2)} \right|$$

$$(58)$$

According to Eqs. (54)–(56) and (58), we have the following inequality formulations regarding $\frac{\partial^2 \Gamma}{\partial u_i(p_1)u_i(p_2)}$, $\frac{\partial^2 \Gamma}{\partial u_i(p_1)u_{i-1}(p_2)}$, $\frac{\partial^2 \Gamma}{\partial u_i(p_1)u_{i-1}(p_2)}$ in Eq. (59).

$$\left| \frac{\partial^{2} \Gamma}{\partial u_{i}(p_{1})u_{i+1}(p_{2})} \right| < \left| \frac{\partial^{2} \Gamma}{\partial u_{i}(p_{1})u_{i}(p_{2})} \right|$$

$$\left| \frac{\partial^{2} \Gamma}{\partial u_{i}(p_{1})u_{i-1}(p_{2})} + \frac{\partial^{2} \Gamma}{\partial u_{i}(p_{1})u_{i+1}(p_{2})} \right| < \left| \frac{\partial^{2} \Gamma}{\partial u_{i}(p_{1})u_{i}(p_{2})} \right|$$

$$\left| \frac{\partial^{2} \Gamma}{\partial u_{i}(p_{1})u_{i-1}(p_{2})} \right| < \left| \frac{\partial^{2} \Gamma}{\partial u_{i}(p_{1})u_{i}(p_{2})} \right|$$
(59)

Based upon Eqs. (53) and (59), we thus have $||B_{i,p}|| < 1$, $i \in N$, $p \in P$ Hence, we know that 1-norm of every row in matrix $I - (\overline{K})^{-1}K$ is smaller than 1, mathematically $||I - (\overline{K})^{-1}K|| < 1$. Finally, we apply the induced norm theorem and obtain

$$\rho^* = \rho \left(I - (\overline{K})^{-1} K \right) \le \parallel I - (\overline{K})^{-1} K \parallel < 1.$$

Condition (III) is satisfied. We conclude the proof.

In summary, Lemma 3 demonstrates our MPC controllers satisfies the three conditions given in Theorem 3. Then Theorem 3 confirms that using the AS-OCD algorithm can efficiently solve the MPC controllers in this study and obtain the global optimal solution with a linear convergence rate. In particular, the approximation of the KKT matrix K in Eq. (47) by \overline{K} in Eq. (48) will not affect the solution optimality and convergence speed.

7. Conclusion

Advanced connected and autonomous vehicle (CAV) technology offers new opportunities for eco-driving strategies at signalized intersections by leveraging traffic signal phase and timing (SPaT) information. The existing eco-driving strategies mainly provide vehicle-level speed plan or advisory for individual vehicles without considering other vehicles' benefits. Although showing improvement in fuel consumption and emissions, these approaches may sacrifice the traffic system performance and lack robustness to various uncertainties in the real world. To bridge these limits, Part I (Zhang and Du, 2022) of this study developed a system optimal platoon-centered control for eco-driving (PCC-eDriving), which provides feedback control law for a mixed flow platoon to pass the signalized intersections smoothly and efficiently. We carefully designed a hybrid MPC system to instruct the entire intersection passing process, which includes the platoon approaching the intersection, then splitting into sub-platoons and sequentially passing the intersection in different traffic cycles. The hybrid MPC system mainly uses three MPC controllers and one mixed integer nonlinear programming switching signal, aiming to generate robust, feasible, and stable control law for the PCC-eDriving. By conducting simulated numerical experiments, Part I demonstrates the merits of the hybrid MPC system. Part II paper theoretically analyzed and proved the control law generated by the hybrid MPC system is feasible, stable, and thus robust. Specifically, we proved the sequential feasibility of the MPC controllers and switching feasibility of the hybrid system, and analyzed how the prediction horizon affects the feasibility of the optimizer. We investigated the asymptotic stability of the nominal MPC controller and further proved the Input-to-State stability of the robust MPC controller in the hybrid MPC system. To ensure satisfying computation performance for this real-time control, Part I of this study designed the AS-OCD algorithm to solve the large-scale MPC optimizers in a distributed manner. Part II of this study moved forward and theoretically proved the convergence and optimality of the AS-OCD algorithm. We conclude that the AS-OCD algorithm can reach the global optimal solution in linear convergence rate when it is used to solve the MPC controllers in this study.

Acknowledgments

This research is partially funded by National Science Foundation, award CMMI 1901994.

Appendix

Appendix A1. Mathematical derivations of Eqs. (38)-(40)

According to the control dynamics in Eqs. (10)–(13) and CAV dynamics in Eqs. (2)–(4), we can have the following mathematical derivations of the CAV i's control dynamics in the Eqs. (60) and (61). Note that we denote $a_i(k) = u_i(k) - \Delta u_i(k)$ for notation simplicity.

$$z_{i}(k+1) = x_{i-1}(k+1) - x_{i}(k+1) - s_{i}(k+1)$$

$$= x_{i-1}(k) - x_{i}(k) + \tau(v_{i-1}(k) - v_{i}(k)) + \frac{\tau^{2}}{2}(a_{i-1}(k) - a_{i}(k)) - s_{i}(k+1)$$

$$= z_{i}(k) + s_{i}(k) - s_{i}(k+1) + \tau z_{i}^{'}(k) + \frac{\tau^{2}}{2}(a_{i-1}(k) - a_{i}(k))$$

$$= z_{i}(k) + \tau z_{i}^{'}(k) - \delta_{1}\tau^{2}a_{i}(k) - \delta_{2}\tau^{2}(a_{i-1}(k) - a_{i}(k)) + \frac{\tau^{2}}{2}(a_{i-1}(k) - a_{i}(k))$$

$$= z_{i}(k) + \tau z_{i}^{'}(k) + \tau^{2}\left(\frac{1}{2} + \delta_{2}\right)a_{i-1}(k) - \tau^{2}\left(\delta_{1} + \delta_{2} + \frac{1}{2}\right)a_{i}(k)$$

$$z_{i}^{'}(k+1) = v_{i-1}(k+1) - v_{i}(k+1)$$

$$= v_{i-1}(k) + \tau a_{i-1}(k) - (v_{i}(k) + \tau a_{i}(k))$$

$$= z_{i}^{'}(k) + \tau(a_{i-1}(k) - a_{i}(k))$$
(61)

Let $c_1 = \delta_2 + \frac{1}{2}$; $c_2 = -(\delta_1 + \delta_2 + \frac{1}{2})$ We have the following Eq. (62) according to Eqs. (60) and (61).

H. Zhang and L. Du

$$\begin{bmatrix} z_i(k+1) \\ z_i'(k+1) \end{bmatrix} = \begin{bmatrix} 1 & \tau \\ 0 & 1 \end{bmatrix} \begin{bmatrix} z_i(k) \\ z_i'(k) \end{bmatrix} + \begin{bmatrix} \tau^2 c_1 & \tau^2 c_2 \\ \tau & -\tau \end{bmatrix} \begin{bmatrix} a_{i-1}(k) \\ a_i(k) \end{bmatrix}$$
(62)

According to the control dynamics of CAV i in Eq. (62), we can then derive out the following platoon control dynamics in Eq. (63),

$$\begin{bmatrix} z(k+1) \\ z'(k+1) \end{bmatrix} = \begin{bmatrix} I_N & \tau I_N \\ 0 & I_N \end{bmatrix} \begin{bmatrix} z(k) \\ z'(k) \end{bmatrix} + \begin{bmatrix} \tau^2 S_1 \\ \tau S_2 \end{bmatrix} a(k)$$
(63)

where $a(k) = \begin{bmatrix} a_0(k) & \dots & a_i(k) & \dots & a_N(k) \end{bmatrix}^T \in \mathbb{R}^{N+1}$ and the matrices S_1 and S_2 are given below with $c_1 = \delta_2 + \frac{1}{2}$; $c_2 = -(\delta_1 + \delta_2 + \frac{1}{2})$.

$$S_1 = \begin{bmatrix} c_1 & c_2 & & & \\ & c_1 & c_2 & & \\ & & \ddots & \ddots & \\ & & & c_1 & c_2 \end{bmatrix} \in \mathbb{R}^{N \times \ (N+1)}; \ S_2 = \begin{bmatrix} 1 & -1 & & & \\ & 1 & -1 & & \\ & & \ddots & \ddots & \\ & & & 1 & -1 \end{bmatrix} \in \mathbb{R}^{N \times \ (N+1)}$$

Appendix A2. The mathematical formulations of \overline{K}_i , $\overline{\Delta}_i$, f_i are presented as follows according to Eqs. (47) and (48)

$$\overline{K}_{i} = \begin{bmatrix} \frac{\partial^{2} L_{AS}(u, \eta, \lambda)}{\partial u_{i}^{2}} & \frac{\partial^{T} c_{i}(u_{i})}{\partial u_{i}} & \frac{\partial^{T} g_{i}(u_{i-1}, u_{i})}{\partial u_{i}} \\ \frac{\partial c_{i}(u_{i})}{\partial u_{i}} & 0 & 0 \\ \frac{\partial g_{i}(u_{i-1}, u_{i})}{\partial u_{i}} & 0 & 0 \end{bmatrix}; \overline{\Delta}_{i} = \begin{bmatrix} \Delta u_{i} \\ -\Delta \eta_{i} \\ -\Delta \lambda_{i} \end{bmatrix}; f_{i} = \begin{bmatrix} \frac{\partial L_{AS}(u, \eta, \lambda)}{\partial u_{i}} \\ c_{i}(u_{i}) \\ g_{i}(u_{i-1}, u_{i}) \end{bmatrix}$$

References

Bof, N., Carli, R. and Schenato, L., 2018. Lyapunov theory for discrete time systems. arXiv preprint arXiv:1809.05289.

Boyd, S., Boyd, S.P., Vandenberghe, L., 2004. Convex Optimization. Cambridge university press.

Chen, C., Wang, J., Xu, Q., Wang, J., Li, K., 2021. Mixed platoon control of automated and human-driven vehicles at a signalized intersection: dynamical analysis and optimal control. Transport. Res. Part C 127, 103138.

Conejo, A.J., Nogales, F.J., Prieto, F.J., 2002. A decomposition procedure based on approximate Newton directions. Math. Program. 93 (3), 495–515.

Gong, S., Shen, J., Du, L., 2016. Constrained optimization and distributed computation based car following control of a connected and autonomous vehicle platoon. Transport. Res. Part B 94, 314–334.

Gong, S., Du, L., 2018. Cooperative platoon control for a mixed traffic flow including human drive vehicles and connected and autonomous vehicles. Transport. Res. Part B 116, 25–61

Greub, W.H., 2012. Linear Algebra. Springer Science & Business Media (Vol. 23).

Kamal, M.A.S., Mukai, M., Murata, J., Kawabe, T., 2012. Model predictive control of vehicles on urban roads for improved fuel economy. IEEE Trans. Control Syst. Technol. 21 (3), 831–841.

Li, X., Cui, J., An, S., Parsafard, M., 2014. Stop-and-go traffic analysis: theoretical properties, environmental impacts and oscillation mitigation. Transp. Res. Part B 70, 319–339.

Lioris, J., Pedarsani, R., Tascikaraoglu, F.Y., Varaiya, P., 2016. Doubling throughput in urban roads by platooning. IFAC-PapersOnLine 49 (3), 49-54.

Löfberg, J., 2012. Oops! I cannot do it again: testing for recursive feasibility in MPC. Automatica 48 (3), 550-555.

Lu, X.Y., Shladover, S.E., 2014. Review of variable speed limits and advisories: theory, algorithms, and practice. Transp. Res. Rec. 2423 (1), 15–23.

Ma, J., Li, X., Shladover, S., Rakha, H.A., Lu, X.Y., Jagannathan, R., Dailey, D.J., 2016. Freeway speed harmonization. IEEE Trans. Intell. Vehicles 1 (1), 78–89. Ma, J., Li, X., Zhou, F., Hu, J., Park, B.B., 2017. Parsimonious shooting heuristic for trajectory design of connected automated traffic part II: computational issues and optimization. Transport. Res. Part B 95, 421–441.

Ma, F., Yang, Y., Wang, J., Li, X., Wu, G., Zhao, Y., Wu, L., Aksun-Guvenc, B., Guvenc, L., 2021. Eco-driving-based cooperative adaptive cruise control of connected vehicles platoon at signalized intersections. Transportat. Res. Part D 92, 102746.

Mayne, D.Q., Rawlings, J.B., Rao, C.V., Scokaert, P.O., 2000. Constrained model predictive control: stability and optimality. Automatica 36 (6), 789–814. Mhaskar, P., El-Farra, N.H., Christofides, P.D., 2005. Predictive control of switched nonlinear systems with scheduled mode transitions. IEEE Trans. Autom. Control 50 (11), 1670–1680.

Newell, G.F., 2002. A simplified car-following theory: a lower order model. Transport. Res. Part B 36 (3), 195-205.

Nak, H., Akkaya, Ş., Yumuk, E., 2017. Active set method based model predictive control for a ball and beam system. In: 2017 10th International Conference on Electrical and Electronics Engineering (ELECO). IEEE, pp. 871–875.

Nocedal, J., Wright, S., 2006. Numerical Optimization. Springer Science & Business Media.

Poch, M., Mannering, F., 1996. Negative binomial analysis of intersection-accident frequencies. J. Transp. Eng. 122 (2), 105–113.

Sastry, S., Bodson, M., 2011. Adaptive Control: Stability, Convergence and Robustness. Courier Corporation.

Shen, J., Kammara, E.K.H. and Du, L., 2021. Nonconvex, Fully Distributed Optimization based CAV Platooning Control under Nonlinear Vehicle Dynamics. arXiv preprint arXiv:2104.08713.

Smith, S.W., Kim, Y., Guanetti, J., Li, R., Firoozi, R., Wootton, B., Kurzhanskiy, A.A., Borrelli, F., Horowitz, R., Arcak, M., 2020. Improving urban traffic throughput with vehicle platooning: theory and experiments. IEEE Access 8, 141208–141223.

Simchon, L., Rabinovici, R., 2020. Real-time implementation of green light optimal speed advisory for electric vehicles. Vehicles 2 (1), 35-54.

ARTICLE IN PRESS

H. Zhang and L. Du

Transportation Research Part B xxx (xxxx) xxx

Sohrab, H.H., 2003. Basic Real Analysis. Birkhäuser, Boston, Basel, Berlin (Vol. 231).

Summala, H., 2007. Towards understanding motivational and emotional factors in driver behaviour: Comfort through satisficing. Modelling Driver Behaviour in Automotive Environments. Springer, London, pp. 189–207.

Treiber, M., Hennecke, A., Helbing, D., 2000. Congested traffic states in empirical observations and microscopic simulations. Phys. Rev. E 62 (2), 1805.

Wan, N., Vahidi, A., Luckow, A., 2016. Optimal speed advisory for connected vehicles in arterial roads and the impact on mixed traffic. Transport. Res. Part C 69, 548–563.

Wang, Z., Wu, G., Barth, M.J., 2019. Cooperative eco-driving at signalized intersections in a partially connected and automated vehicle environment. IEEE Trans. Intell. Transp. Syst. 21 (5), 2029–2038.

Wiedemann, R., 1991. Modelling of RTI-Elements on multi-lane roads. In: Drive Conference (1991: Brussels, Belgium) (Vol. 2).

Zeilinger, M.N., Jones, C.N., Raimondo, D.M., Morari, M., 2009. Real-time MPC-stability through robust MPC design. In: Proceedings of the 48h IEEE Conference on Decision and Control (CDC) held jointly with 2009 28th Chinese Control Conference. IEEE, pp. 3980–3986.

Zhang, H., Du, L., Shen, J., 2022. Hybrid MPC system for platoon based cooperative lane change control using machine learning aided distributed optimization. Transport. Res. Part B 159, 104–142.

Zhang, H., Du, L., 2022 Feasibility Analysis and Proof of Model Predictive Control, arXiv, arXiv.2206.11439.

Zhao, W., Ngoduy, D., Shepherd, S., Liu, R., Papageorgiou, M., 2018. A platoon based cooperative eco-driving model for mixed automated and human-driven vehicles at a signalised intersection. Transport. Res. Part C 95, 802–821.1